Review | Open Access

Energy Materials

Yang *et al. Energy Mater.* **2026**, *6*, 600160 **DOI:**10.20517/energymater.2026.146

Site engineering of spinel electrocatalysts for water oxidation: from bulk modulation to confined interfaces

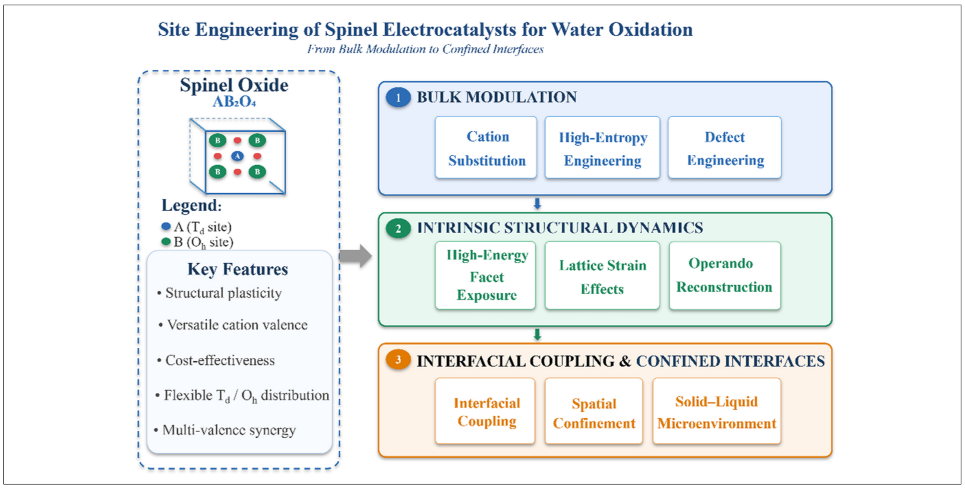
Bing Yang[1,#], Enze Zhu[1,*,#], Haoran Jia[1], Yifan Wang[1], Bing-Xin Lei[1,*], Zhao-Qing Liu[2,3,*]

Keywords:
Oxygen evolution reaction, spinel oxides, site engineering, bulk modulation, interfacial coupling

Citation: Yang, B.; Zhu, E.; Jia, H.; Wang, Y.; Lei, B. X.; Liu, Z. Q. Site engineering of spinel electrocatalysts for water oxidation: from bulk modulation to confined interfaces. *Energy Mater.* **2026**, *6*, 600160. https://dx.doi.org/10.20517/energymater.2026.146

Received: 2 Jun 2026
First Decision: 21 Jul 2026
Revised: 26 Oct 2026
Accepted: 5 Nov 2026
Published: 20 Nov 2026

Academic Editor:
Yuhui Chen
Copy Editor:
Ping Zhang
Production Editor:
Ping Zhang



Abstract

Spinel oxides (AB_2O_4) have emerged as widely studied non-noble-metal electrocatalysts for the oxygen evolution reaction owing to their structural plasticity, versatile cationic valence states, and cost-effectiveness. To circumvent the high activation barriers of multi-step proton-coupled electron transfer and improve catalytic efficiency, current research has shifted toward advanced site engineering to precisely orchestrate the catalytic active centers. This review presents a structured framework that organizes site-engineering strategies into three complementary dimensions. At the bulk level, strategic cation substitution, high-entropy-oxide engineering, and defect engineering deeply remodel the d-orbital configurations and metal-oxygen covalency, which can alter lattice-oxygen

[1]School of Materials and Environment, Guangxi Key Laboratory of Advanced Structural Materials and Carbon Neutralization, Guangxi Engineering Research Center for Advanced Materials and Intelligent Manufacturing, Guangxi Minzu University, Nanning 530105, Guangxi, China.
[2]School of Chemistry and Chemical Engineering/Institute of Clean Energy and Materials/Key Laboratory for Clean Energy and Materials, Guangzhou University, Guangzhou 510006, Guangdong, China.
[3]School of Chemistry, South China Normal University, Guangzhou 510006, Guangdong, China.
[#]These authors contributed equally to this work.

[*]**Correspondence to:** Dr. Enze Zhu, Prof. Bing-Xin Lei, School of Materials and Environment, Guangxi Key Laboratory of Advanced Structural Materials and Carbon Neutralization, Guangxi Engineering Research Center for Advanced Materials and Intelligent Manufacturing, Guangxi Minzu University, Nanning 530105, Guangxi, China. E-mail: zhuenze@gxmzu.edu.cn; leibx@gxmzu.edu.cn; Prof. Zhao-Qing Liu, School of Chemistry and Chemical Engineering/Institute of Clean Energy and Materials/Key Laboratory for Clean Energy and Materials, Guangzhou University, Guangzhou 510006, Guangdong, China; School of Chemistry, South China Normal University, Guangzhou 510006, Guangdong, China. E-mail: lzqgzu@gzhu.edu.cn

reactivity and may help reduce activity limitations under selected conditions. At the surface level, we examine high-energy-facet exposure, lattice-strain effects, and operando reconstruction, which may generate catalytically relevant oxyhydroxide species in selected systems and influence interfacial kinetics. Finally, built-in electric fields at coupled interfaces can promote charge redistribution, while genuine spatial confinement and molecular-level control over the solid-liquid microenvironment can improve interfacial transport and intermediate regulation. By synthesizing these multi-scale strategies, this review proposes an organizing framework for the rational design of next-generation, highly efficient electrocatalysts for the oxygen evolution reaction.

INTRODUCTION

The global transition toward clean, low-carbon energy systems has positioned hydrogen-based renewable energy networks as a cornerstone for achieving carbon neutrality[1]. The anodic oxygen evolution reaction (OER) is central to these technologies, as it dictates the overall energy efficiency of water electrolysis[2]. While noble metal oxides such as IrO_2 exhibit excellent intrinsic activities, their scarcity and prohibitive costs preclude large-scale industrial application. Consequently, the development of high-performance, low-cost non-precious-metal catalysts has become a central goal for both academia and industry.

As a complex four-electron transfer process involving multi-step proton-coupled electron transfer, the OER has high activation energy barriers that fundamentally limit performance[3]. To overcome this bottleneck, current research focuses on three primary catalytic pathways: the adsorbate evolution mechanism (AEM), the lattice oxygen mechanism (LOM), and the oxide path mechanism (OPM)[4]. The AEM involves the sequential adsorption and dissociation of oxygenated intermediates (*OH, *O, and *OOH) on active metal sites. The LOM involves lattice-oxygen participation and may alter the conventional adsorbate-scaling constraint under specific conditions. The OPM has been proposed as an alternative pathway, although its effect on structural stability must be verified for each catalyst [Figure 1][5].

Among the numerous metal catalyst candidates, spinel oxides (AB_2O_4) stand out for their highly symmetric face-centered cubic structures and high structural flexibility. Their crystal lattices accommodate a flexible distribution of metal cations within tetrahedral (T_d) and octahedral (O_h) voids, enabling the formation of normal, inverse, or complex mixed spinel structures[6]. The core scope of this review is phase-pure and chemically modified AB_2O_4 spinel oxides evaluated for water oxidation. Spinel-derived phases and heterostructures are included only when their roles in spinel-based OER are explicitly examined[7]. These systems provide flexible cation distributions and tunable structural and electronic properties for regulating catalytic activity and stability. Heterostructures containing a spinel phase, such as those coupled with CeO_2 or noble metals, are considered where their interfacial effects on OER are specifically investigated[8,9]. In addition, operando surface reconstruction is discussed when it generates oxyhydroxide-like species that contribute to OER activity. The identity, abundance, and catalytic role of these reconstructed species depend on the spinel composition, electrolyte, applied potential, and operating time.

High-entropy spinels can be categorized into low- (configurational entropy < 1.0 *R*), medium- (1.0-1.5 *R*), and high-entropy (> 1.5 *R*) regimes on a per-mole-of-cations basis, where *R* is the ideal gas constant[10]. These thresholds are descriptive rather than universal. Because spinels contain distinct tetrahedral and octahedral cation sublattices, their ideal configurational entropy can be calculated by summing the contributions from the two sublattices[11]. On the same per-mole-of-cations basis, the expression becomes $S_{config} = -\frac{R}{3}\sum_s m_s \sum_i x_{i,s} \ln x_{i,s}$[12], where s denotes the tetrahedral or octahedral sublattice; m_s is the number of site on sublattice s per AB_2O_4 formula unit ($m_{Td} = 1$ and $m_{Oh} = 2$); and $x_{i,s}$ is the normalized occupancy fraction of cation i on sublattice s, with $\sum_i x_{i,s} = 1$. The factor of 1/3 converts the site-weighted entropy per mole of AB_2O_4 formula units to a per-mole-of-cations basis. Cation ordering, local clustering, phase segregation,

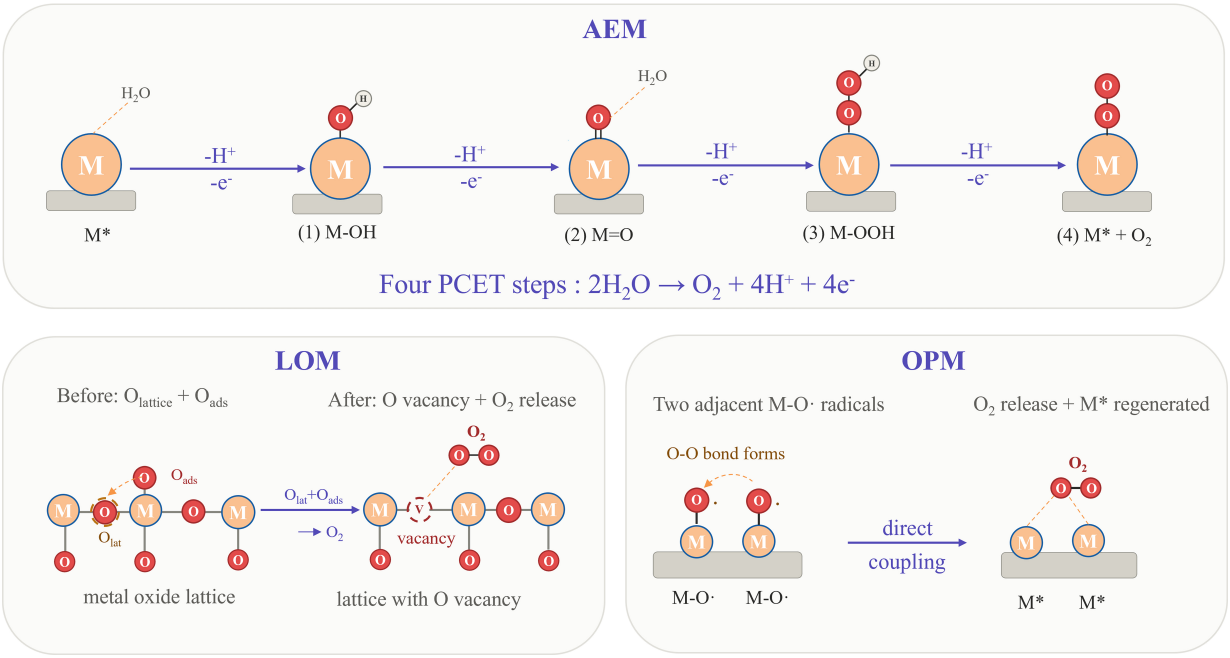


Figure 1. Conceptual schemes of proposed AEM, LOM, and OPM pathways for the oxygen evolution reaction. AEM: Adsorbate evolution mechanism; LOM: lattice oxygen mechanism; OPM: oxide path mechanism; PCET: proton-coupled electron transfer.

vacancies, and non-ideal interactions may cause deviations from the ideal-mixing value. Medium- and high-entropy compositions may enrich local coordination environments and influence OER kinetics, but these effects are system-dependent and should not be attributed solely to multication mixing. The resulting phase stability and catalytic behavior are governed by the balance among configurational entropy, enthalpic interactions, synthesis conditions, local cation distribution, phase purity, and possible elemental segregation or operando demixing. Therefore, structural and compositional characterization is essential before assigning phase stabilization or catalytic enhancement to configurational-entropy effects[13-15]. Recent studies indicate that some spinel oxides can behave as dynamic pre-catalysts[16], undergoing partial surface reconstruction into catalytically relevant metal oxyhydroxide species under anodic polarization. The extent and reversibility of this transformation are system-dependent[17], while the residual spinel may continue to provide structural support, charge transport[18], and elemental reservoirs for the reconstructed surface.

Notably, non-noble-metal spinel oxides are widely studied under alkaline conditions, where their stability is generally more favorable. Their application in acidic environments remains challenging because of anodic dissolution and structural instability, although recent studies have demonstrated that selected non-noble-metal spinel anodes can operate in acidic proton-exchange-membrane water electrolyzers (PEMWE). To address the diverse pH requirements of various electrolysis technologies, this review primarily focuses on the design principles of spinels in alkaline and neutral media while also analyzing recent approaches to overcoming the stability limitations of acidic OER.

The research paradigm is shifting from simple compositional optimization toward systematic site engineering to bridge the gap between atomic-scale structure-activity relationships and reported current-density measurements, including selected electrolyzer demonstrations. This review provides a panoramic overview of this evolution across three complementary dimensions: setting the evolutionary potential at the bulk level, guiding active-phase evolution through intrinsic structural dynamics, and optimizing interfacial processes through interfacial coupling and confined-interface strategies [Figure 2]. A comparison of the

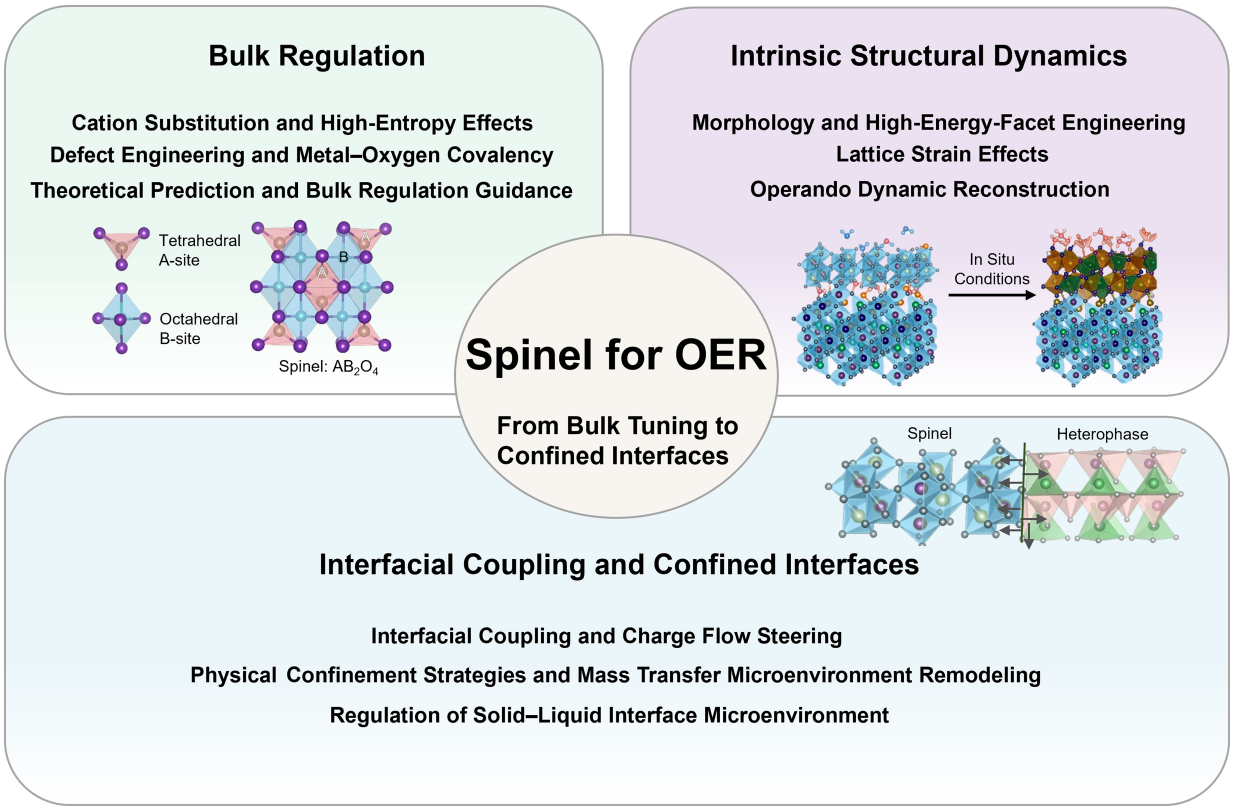


Figure 2. Panoramic landscape of site engineering strategies for AB_2O_4. OER: Oxygen evolution reaction.

scope and core research dimensions of this review with those of previous reviews is provided in Supplementary Table 1. Its distinctive contribution lies in integrating these dimensions into an evidence-qualified cross-scale framework rather than treating individual modification strategies as isolated approaches. First, at the bulk level, we critically examine how the intrinsic electronic structure is remodeled through cation substitution, high-entropy-oxide engineering, and defect engineering, with a focus on assessing how reaction pathways may be affected under selected conditions. Second, we focus on intrinsic structural dynamics, analyzing how the physical and geometric parameters, including the facet exposure, localized lattice strain, and dynamic reconstruction, stabilize the active centers and lower the reaction barriers. Finally, we explore how interfacial coupling through built-in electric fields (BIEFs) and confined-interface strategies based on genuine spatial confinement and microenvironmental regulation provide complementary effects. Through this multi-dimensional perspective, we provide a structured theoretical framework to guide the design of next-generation electrocatalysts capable of efficient and stable operation under application-relevant electrolyzer conditions.

BULK REGULATION AND INTRINSIC REMODELING OF ELECTRONIC STRUCTURE

Bulk regulation is fundamental to site engineering in AB_2O_4. It allows the systematic control of cation substitution and bulk composition. Tailoring the elemental ratios of the bulk phase enables its crystal lattice and electronic structure to be remodeled. The core paradigm of bulk regulation is the introduction of controlled lattice perturbations via precise cation substitution, high-entropy-oxide engineering (achieved through multi-component mixing), and defect engineering (triggered by component deficiencies) to systematically reshape the d-orbital electronic configurations and metal-oxygen (M-O) covalency[19]. Within this framework, strategic cation substitution serves as the primary means to adjust the M-O covalency, which may influence the contribution of different reaction pathways under selected structural and operating

conditions. Because the catalyst is not static, this intrinsic remodeling may accompany changes in operando surface reconstruction and possible contributions from alternative pathways, including LOM, at the dynamically formed active interface, offering a promising strategy to help mitigate the activity-stability trade-off. The majority of previous studies have emphasized activity enhancement, with systematic stability data remaining comparatively limited[20].

Cation substitution and high-entropy effects

Cation substitution provides a direct approach for modulating the crystal-field splitting energy and optimizing the d-orbital electronic configurations of active metal centers[21]. One primary strategy targets O_h sites for spin-state tuning. For example, incorporating Cr^{3+} into Co_3O_4 induces a directional Jahn-Teller distortion within CoO_6 octahedra, triggering a transition of Co sites from a low-spin to an intermediate-spin state ($e_g \approx 1$). This distortion dynamically adjusts the active site spacing to provide optimal geometric configurations for proposed O-O radical coupling, which may reduce the charge-transfer resistance and accelerate the redox kinetics [Figure 3A][22]. Beyond spin-state and defect engineering, cation substitution offers additional design strategies, as discussed below.

A complementary family of strategies exploits indirect electronic effects originating from T_d sites and local bond competition. Trace incorporation of rare-earth elements such as Er, La, or Nd has been reported to modify lattice strain and oxygen-vacancy populations, thereby influencing the local Co electronic structure. These changes may regulate spin and valence states through the rare-earth tetrad effect, providing a means of tuning adsorption energetics and improving OER stability in acidic PEMWE[23-25]. A more direct manifestation of this concept is the rigid T_d-O-O_h bridging network, which functions as an electronic bridge that systematically shifts the d-band center to optimize the intermediate adsorption strength [Figure 3B][26]. This result illustrates a transferable electronic-coupling concept; the reported electronic descriptor does not constitute direct proof of a specific water-oxidation pathway. A further level of sophistication is achieved by introducing elements that compete for bonding within O_h sites[27]. The incorporation of highly electronegative Mn^{3+} into $ZnCo_2O_4$ triggers intense electronic competition between Mn-O and Co-O bonds, inducing local Jahn-Teller distortions that optimize the binding free energies of *OH and *O. This bond-competition strategy was associated with an overpotential of 350 mV for $ZnMn_{1.4}Co_{0.6}O_4$ under the reported testing conditions[28]. Incorporation of Ir into Mn_3O_4 breaks crystallographic symmetry to facilitate oxidative charge accumulation on neighboring Mn atoms, lowering the surface oxidation potential for active species formation[29]. Meanwhile, anchoring isolated Ru atoms at ultralow loading on $Co_2MnO_{4.5}$ induces a localized compressive strain that is consistent with increased OPM participation, effectively suppressing lattice dissolution while enhancing the acidic OER durability[30].

While the bond-competition strategy reshapes the local orbital interactions, the work function engineering approach alters the global electronic properties, demonstrating the versatility of substitutional tuning. A distinct motivation is the suppression of catalyst degradation under harsh operating conditions[31,32]. Using online inductively coupled plasma mass spectrometry to monitor real-time metal dissolution, Liu *et al.* demonstrated that Cu or Mn co-doping effectively inhibits the over-oxidation of O_h metal sites under high polarization, with Mn doping significantly enhancing the resistance of Co-based spinels to degradation during the acidic OER[33]. This strategy differs fundamentally from the spin-state and bond-competition approaches discussed above, as its primary objective is to construct a dissolution-resistant lattice that preserves the active sites over extended operation. Together, these examples trace a coherent progression from electronic structure tuning (spin-state, d-band, or bond competition) through interfacial energetics (work function) to structural integrity (anti-dissolution), each building upon a distinct aspect of the cation substitution landscape.

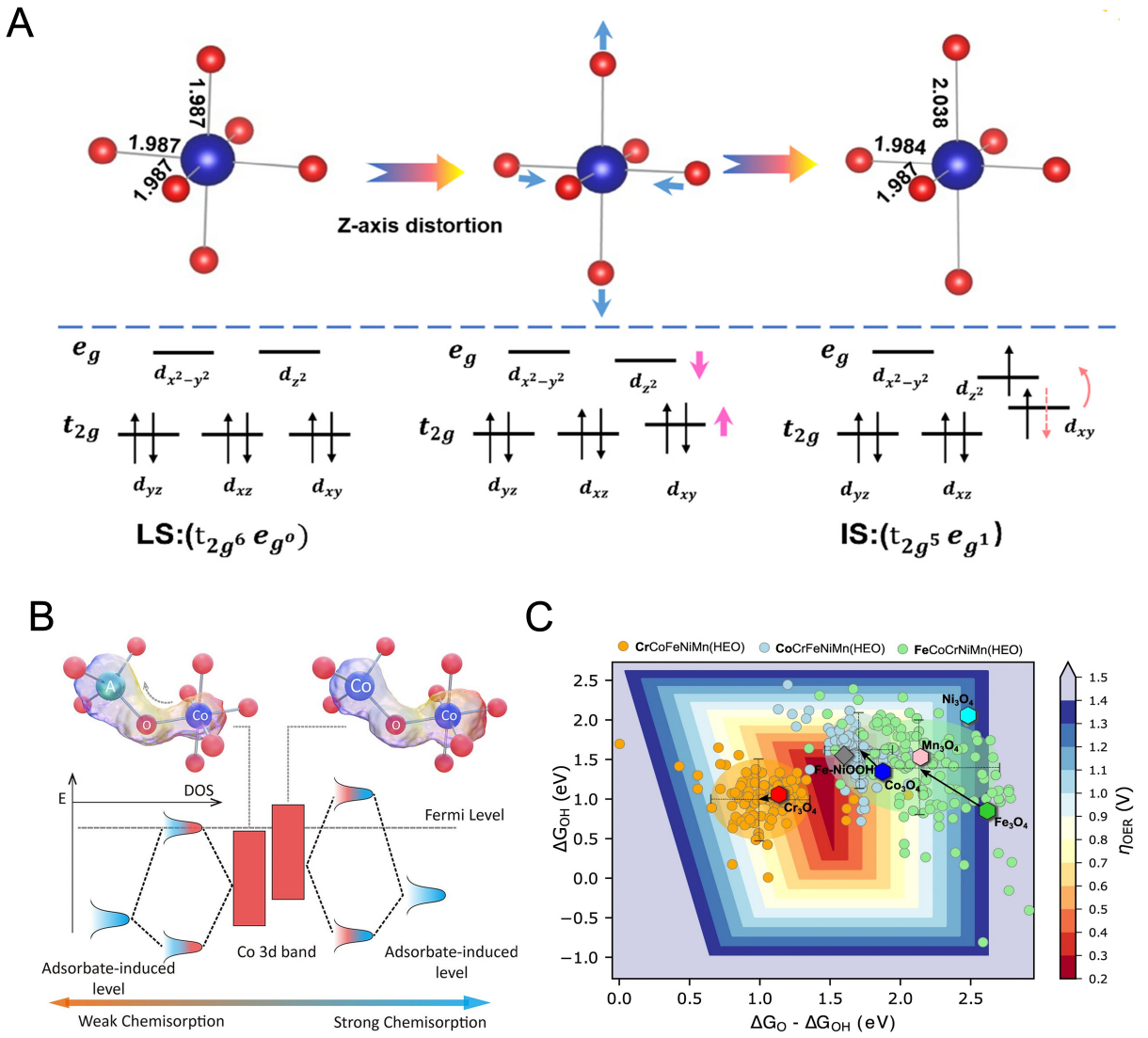


Figure 3. (A) Schematic illustration of the Jahn-Teller-distortion-induced transition from a low-spin to an intermediate-spin state at octahedral (O_h) sites in Cr-doped Co_3O_4. (A) is reproduced with permission from Ref.[22]. Licensed under CC BY 4.0; (B) Electronic structure modulation of octahedral Co via tetrahedral site substitution in the T_d-O-O_h corner-sharing configuration. (B) is reproduced with permission from Ref.[26]. Copyright 2021, Wiley-VCH GmbH; (C) Two-dimensional volcano heat map for OER over high-entropy AB_2O_4: overpotential dependence on *O and *OH binding energies for different active sites (Cr, Co, Fe) and comparison with Fe-NiOOH. (C) is reproduced with permission from Ref.[38]. Licensed under CC BY 4.0. OER: Oxygen evolution reaction; HEO: high-entropy oxide; DOS: density of states.

While the strategies outlined above rely on selective substitution of one or a few cations, a distinct compositional strategy, high-entropy engineering, integrates multiple cations into a single, globally distorted lattice. Incorporating five or more principal metal cations is commonly used as a compositional descriptor, but it does not by itself demonstrate high-entropy stabilization; phase stability, local disorder, lattice distortion, defect formation, and high-valence surface species must be evaluated from composition-specific site occupancies, phase purity, and operando characterization[34,35]. This synergy of multi-element cooperation, lattice distortion, and surface reconstruction can improve OER performance in selected systems, as demonstrated by nanosized $(FeCoNiCrMn)_3O_4$, which achieved an overpotential of 239 mV at 10 mA cm^{-2} under the reported test conditions[36]. The complex microenvironments in high-entropy systems have also been reported to exhibit moisture tolerance under the tested conditions[37].

Furthermore, the micro-strains inherent to high-entropy systems induce periodic fluctuations in the M-O bond length, which, in synergy with multi-valence mechanisms, may influence the reported electrochemical behavior. The mixing of multiple cations in high-entropy spinel oxides creates chemically diverse local environments and leads to variations in the adsorption energies of OER intermediates. These variations result in distinct distributions of calculated active-site activities and overpotentials for Cr-, Co-, and Fe-containing sites, as illustrated by the two-dimensional OER volcano/overpotential heat map based on the high-entropy-oxide impurity models calculated by Baek *et al.* [Figure 3C][38]. This concept can be extended to real extreme environments by combining defect-rich high-entropy spinels, which may provide structural stability, with O-vacancy engineering, which may modify chloride interactions. Under the reported conditions, OER Faradaic efficiency was quantified by gas-volume measurement, while chlorine and hypochlorite were assessed separately by Na_2S trapping and iodide titration, respectively[39]. Although chlorine and hypochlorite were not detected by these methods under the reported conditions, the detection limits were not reported. Thus, the high-entropy approach represents a strategy that differs from selective cation substitution by jointly modifying multiple electronic and geometric variables, which may provide additional opportunities for tuning OER performance.

Defect engineering and M-O covalency

Defect engineering introduces structural imperfections, such as anion or cation vacancies, to disrupt the local symmetry and expose coordinatively unsaturated active sites. The physical basis of this approach is a redistribution of local electron density that remodels the M-O covalency and can alter local coordination and electronic structure and, in selected systems, may be associated with alternative pathway contributions[40-43].

Beyond modifying local coordination and electronic properties, defect engineering can also be combined with hetero-element doping to regulate OER pathways. Mo-doped Co_3O_4 provides an example in which dopant incorporation induces O vacancies and enhances Co 3d-O 2p orbital overlap, strengthening the M-O covalency to suppress detrimental lattice-oxygen oxidation under acidic conditions while simultaneously optimizing Co-site spacing for direct O-O bond formation. *In situ* Fourier-transform infrared (FTIR) spectroscopy detected O-O-related intermediates, providing evidence consistent with OPM participation; however, the exclusivity of this pathway requires further verification[44].

The LOM represents a different mechanistic outcome, in which vacancy-induced changes may enable lattice-oxygen participation[45,46]. Fe-doping-induced cation substitution and anion vacancies in Co_3O_4 hexagonal nanosheets have been reported to increase lattice-oxygen reactivity and are consistent with a possible LOM contribution for efficient overall water splitting[47]. In a further demonstration, the controllable introduction of metal vacancies in $ZnFe_2O_4$ was interpreted as evidence consistent with increased lattice-oxygen reactivity[48], based on a significant upshift of the O p-band center, which was reported to strengthen *O binding. However, this observation does not establish an AEM-to-LOM transition. The catalyst delivered an overpotential of 236 mV at 10 mA cm^{-2} in alkaline electrolyte. Thus, even within the same broad category of vacancy engineering, different mechanistic interpretations, including OPM and LOM, have been proposed depending on whether the electronic restructuring primarily optimizes metal-site spacing or activates lattice O, highlighting the need to relate defect design to hypothesized pathways through operando validation.

However, the high covalency associated with increased lattice-oxygen reactivity can be a double-edged sword, predisposing the catalyst to lattice O depletion and metal dissolution. Several strategies have been developed to precisely modulate the covalency and decouple the activity from the stability. At the anion level, filling O vacancies in $ZnCo_2O_4$ with fluorine was reported to modify the vacancy environment and M-O covalency. The enhanced M-O covalency facilitates the transition toward the LOM mechanism. The closer the O 2p band center shifts upward to the Fermi level, the stronger the orbital hybridization between metal d

and oxygen p states (M-O covalency), and the more favorable the LOM pathway [Figure 4A]. The reported pH dependence and chemical-probe results support enhanced lattice-oxygen involvement, although the evidence remains indirect[49]. At the cation level, Ru substitution into the Td sites of Co_3O_4 has been associated with increased lattice-oxygen reactivity and a possible LOM contribution and suppresses the dissolution of active Co species[50]. *In situ* ^{18}O-labeling combined with differential electrochemical mass spectrometry provides direct evidence for lattice-oxygen-derived oxygen species under the reported test conditions. A comparison of these two approaches reveals that fluoride incorporation primarily stabilizes the lattice framework from within, whereas Ru substitution at remote T_d sites modulates covalency. Both approaches have been associated with increased lattice-oxygen reactivity, although the evidentiary strength differs between the two systems. A synergistic approach goes a step further by combining high-valence centers with metal vacancies. Incorporating both Ni^{4+} centers and Ni vacancies at the octahedral sites of $NiFe_2O_4$ enhanced the M-O covalency in the pristine and reconstructed phases, yielding an overpotential of 293 mV at 500 mA cm^{-2}[51]. This strategy, which involves adding a high-valence cation to further strengthen the covalency, contrasts with the metal vacancy approach in $ZnFe_2O_4$, thereby illustrating how the integration of multiple defect types can amplify performance through an additive effect on electronic restructuring.

Mechanistic evidence in this Review is classified into three levels: Level I, theoretical predictions or correlations; Level II, indirect experimental evidence that is consistent with, but does not uniquely establish, the proposed pathway; and Level III, strong evidence for pathway assignment from isotope labeling, differential electrochemical mass spectrometry (DEMS), online electrochemical mass spectrometry (OEMS), or pathway-specific operando characterization. Mechanistic conclusions are qualified according to the evidence level and the limitations of the corresponding measurements under the tested conditions [Table 1].

Conversely, in specific environments where the structural integrity is paramount, a moderate reduction in the covalency is crucial for longevity. Incorporating approximately 30% Fe into both the T_d and O_h sites of Co spinel decreased the M-O covalency, raising the energy barriers for over-oxidation in the neutral-pH OER and preventing structural collapse[52]. Similarly, doping Co-Mn spinels with bromine anions with large ionic radii has been shown to suppress spontaneous O vacancy formation, stabilizing the active Co centers and enabling stable OER under acidic conditions for over 100 h at 100 mA cm^{-2}[53]. These examples demonstrate that tuning the covalency is not unidirectional, as high covalency has been associated with increased activity and possible LOM or OPM contributions in selected systems, while a deliberately weakened covalency ensures stability in corrosive or neutral environments. A balance between activity and stability may be achieved by jointly optimizing oxidation states and M-O covalency within a robust structural framework. This was demonstrated by Cr-doped Co_3O_4, where a strengthened Co-O covalency and a high initial Co oxidation state facilitated water adsorption and intermediate evolution, enabling stable operation at a current density of 1,500 mA cm^{-2} while operating at 2.17 V in a PEMWE [Figure 4B][54]. This progressive modulation of covalency, from enhancement for activity through controlled weakening for stability to achieving a synergistic balance, captures the evolving design logic in defect engineering.

Theoretical prediction and bulk regulation guidance

The vast compositional space of spinels and the thermodynamic activity-stability trade-off necessitate the integration of theoretical calculations and machine learning (ML) for predictive design. High-throughput density functional theory screening, combined with ML, has identified key electronic descriptors. Guided by the "computation first, experiment second" principle, a five-step high-throughput pipeline was developed to accelerate catalyst discovery [Figure 4C][55]. First, a virtual material library encompassing 6,155 ternary-phase spinel oxides with the general formula $A_xB_{3-x}O_4$ (x = 0.5, 1 and 1.5, where A and B are two different metallic elements) was constructed from 52 metal elements, covering alkaline, alkaline-earth, transition (with the

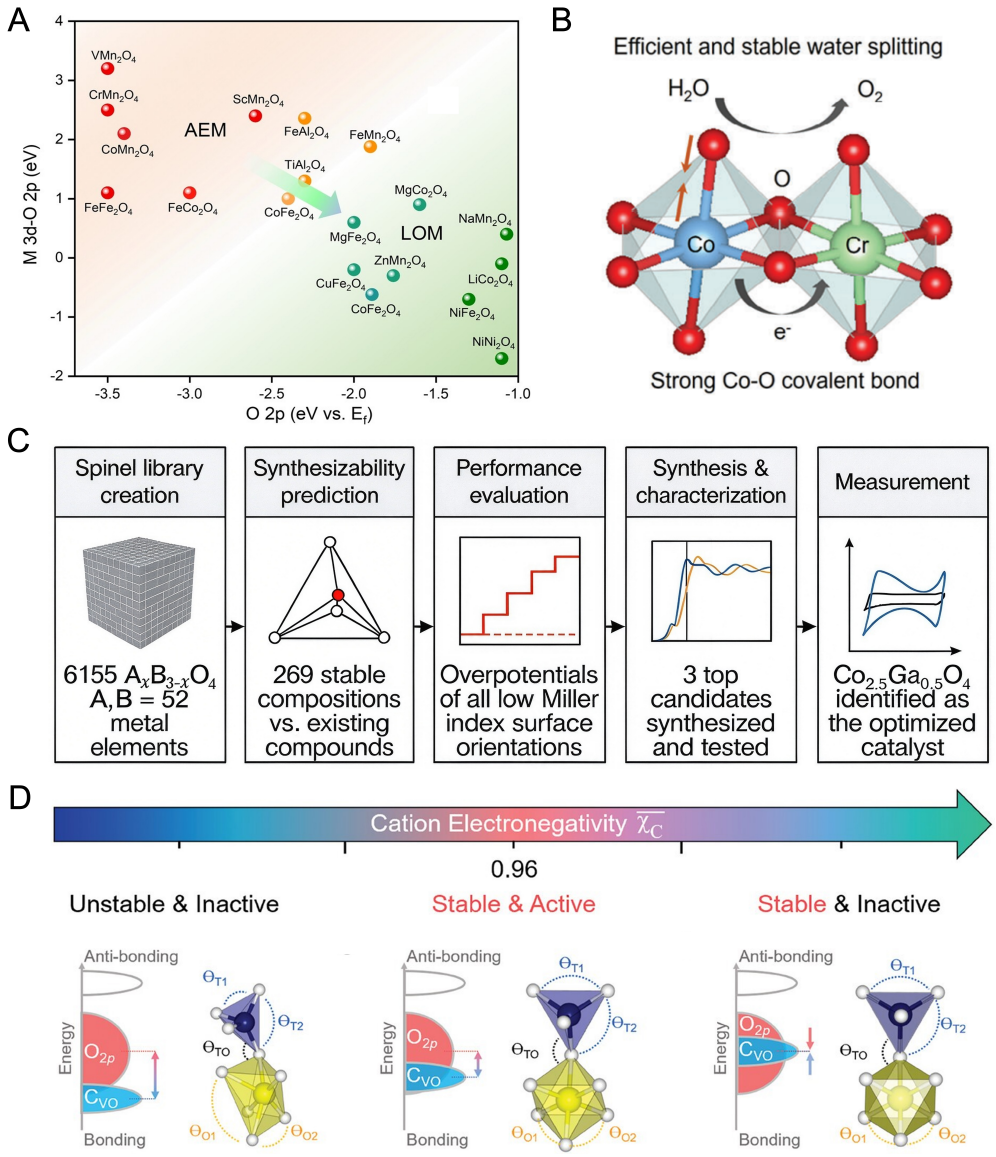


Figure 4. (A) Schematic relationship between OER mechanism (AEM *vs.* LOM) and the relative positions of metal 3d and oxygen 2p band centers in AB_2O_4. (A) is reproduced with permission from Ref.[49]. Copyright 2023, Wiley-VCH GmbH; (B) Schematic diagram of strengthened Co-O covalent bonding in Cr-substituted spinel Co_3O_4. (B) is reproduced with permission from Ref.[54]. Licensed under CC BY 4.0; (C) High-throughput workflow for computational screening of novel spinel-oxide OER catalysts. (C) is adapted with permission from Ref.[55]. Licensed under CC BY 3.0; (D) Design principle of spinel oxide electrocatalysts: predicted stability and catalytic activity as a function of the covalency indicator $\overline{\chi_C}$ (weighted average cation electronegativity). (D) is reproduced with permission from Ref.[56]. Licensed under CC BY-NC-ND 4.0. OER: Oxygen evolution reaction; AEM: adsorbate evolution mechanism; LOM: lattice oxygen mechanism.

exception of artificial Tc) and post-transition metals, as well as five lanthanide elements (La, Ce, Nd, Gd and Lu). Second, thermodynamic stability predictions drastically narrowed the candidate pool down to 269 stable phases. Third, systematic evaluation of the electrochemical overpotentials across all low-Miller-index facets isolated the top three candidates. Fourth, these three targeted compositions were precisely synthesized and structurally verified in the laboratory. Finally, $Co_{2.5}Ga_{0.5}O_4$ showed the lowest overpotential among the tested candidates, with a value of 220 mV at 10 mA cm^{-2}. Despite the promise of ML-assisted materials discovery, prediction reliability is affected by data provenance, duplicated records, heterogeneous testing conditions, inconsistent electrochemical labels, and possible data leakage. Uncertainty quantification, out-of-domain assessment, synthetic feasibility, and experimental validation are therefore essential for evaluating

Table 1. Proposed pathway schemes and evidence hierarchy for spinel-based OER catalysts

Catalyst	Proposed pathway	Diagnostic method	Primary observation	Alternative interpretation	Evidence level	Conclusion permitted by the evidence	Ref.
Mo-doped Co_3O_4	OPM contribution	*In situ* FTIR spectroscopy	O-O-related intermediates	Overlapping oxygenated surface species	Level II	Supports possible OPM participation	[44]
$ZnFe_2O_4$ with metal vacancies	LOM contribution	O 2p band analysis and electrochemical data	O 2p upshift and enhanced *O binding	Modified adsorption energetics without lattice-oxygen turnover	Level I-II	Suggests increased lattice-oxygen reactivity	[48]
F-filled $ZnCo_2O_4$	LOM contribution	pH dependence and chemical probes	Response consistent with lattice-oxygen involvement	Surface hydroxylation or electrolyte effects	Level II	Supports, but does not prove, LOM participation	[49]
Ru-substituted Co_3O_4	LOM contribution	^{18}O labeling and DEMS	Detection of lattice-oxygen-derived oxygen species	Surface-adsorbed oxygen species or near-surface oxygen scrambling	Level III	Directly supports lattice-oxygen participation under the tested conditions	[50]

OER: Oxygen evolution reaction; OPM: oxide path mechanism; LOM: lattice oxygen mechanism; FTIR: Fourier-transform infrared; DEMS: differential electrochemical mass spectrometry.

ML-derived candidates.

While this workflow efficiently screens for activity, a parallel theoretical effort has focused on quantifying the activity-stability trade-off through a covalency indicator, $\overline{\chi C} = (\chi_A + 2\chi_B)/3$, where χ_A and χ_B are the Pauling electronegativities of the A- and B-site cations, respectively; division by three normalizes the site-weighted value to the total cation-site stoichiometry. This index provides a composition-based proxy for covalency: higher $\overline{\chi_C}$ values correspond to a smaller cation-oxygen electronegativity difference and stronger estimated covalency. Within the computed set of 515 metallic cubic Fd-3m spinel candidates, an optimal threshold of $\overline{\chi_C} \approx 0.96$ was identified as a model-specific threshold associated with the activity-stability trade-off within the modeled composition domain [Figure 4D][56]. Its applicability should be limited to the modeled composition domain and should not be assumed across electrolytes or reconstructed active phases. The two theoretical frameworks are complementary: one prioritizes activity prediction, while the other explicitly incorporates stability constraints. Thus, their combined application provides a more holistic screening paradigm.

Moving deeper, the principle of covalency competition between T_d and O_h sites has emerged as an important factor influencing OER activity. ML screening based on this principle identified a Mn-Al spinel as a computationally promising candidate for OER. The predicted activity of $Al_{0.5}Mn_{2.5}O_4$ was subsequently evaluated experimentally using synthesized $Al_{0.5}Mn_{2.5}O_4$, providing experimental support for the computational prediction[57]. Subsequently, interpretable deep learning based on center-environment features was used to map multi-shell electron delocalization across 5,329 spinels, with $MoAg_2O_4$ identified as a computationally predicted composition with a potentially favorable local electronic environment for OER, although experimental validation has not yet been reported[58]. These studies illustrate the logical progression from activity-centric screening to the incorporation of structural stability descriptors and eventually to the identification of a potentially favorable electronic environment. Furthermore, first-principles calculations have addressed the thermodynamic driving force for surface reconstruction, demonstrating that the covalency polarization between T_d and O_h sites may influence the preferred spatial reorganization of atoms in the modeled systems to minimize the surface energy. Weaker bonds undergo displacement, providing a descriptor for a possible reconstructed surface configuration under reaction conditions[59]. This body of work

illustrates an evolution in theoretical guidance, from compositional screening to the quantitative description of competitive electronic interactions and, ultimately, to predicting phase evolution, suggesting a computational-to-experimental workflow for future validation.

INTRINSIC STRUCTURAL DYNAMICS

Electrocatalytic reactions are fundamentally interfacial charge-transfer processes. Intrinsic structural dynamics links bulk-level descriptors to interfacial kinetics under operating conditions. Synergistically managing facet-dependent site exposure, lattice strain, and the operando evolution of active (oxy)hydroxide layers may help connect bulk descriptors with interfacial catalytic behavior. The theoretical activity limits established through bulk modulation must therefore be realized through the precise reshaping of surface and interfacial physicochemical properties, translating intrinsic advantages into macroscopic performance[60,61].

Morphology and high-energy-facet engineering

Engineering the static geometric and electronic structures, from mesoscopic morphologies to atomic-level facets, is a prerequisite for maximizing active-site exposure. Mesoscale engineering constructs 3D porous or hierarchical architectures such as nanoflower and nanoneedle arrays, exponentially expanding the electrochemical surface area and shortening the diffusion paths for ions and gas bubbles[62,63]. However, the polycrystalline nature of such architectures often obscures atomic-scale structure-activity relationships. This limitation was addressed by studies of single-crystal epitaxial thin films, which showed that the (001) facet is the most active for Co_3O_4, whereas $CoFe_2O_4$ and Fe_3O_4 are dominated by the (111) facet [Figure 5A][64]. This facet-specific behavior establishes a geometric benchmark that complements mesoscale engineering by revealing which crystal orientations should be preferentially exposed. Additionally, scaling the catalyst dimensions to the quantum dot level represents a distinct strategy that is not reliant on facet selection. In 2.8 nm Co_3O_4 quantum dots, significant lattice expansion was found to increase the Co-O bond length, optimizing intermediate adsorption kinetics[65]. Integrating this size effect with surface hydroxylation (Co_3O_4-OH) yielded an overpotential of 293 mV and maintained stable catalytic performance for 240 h. Thus, facet engineering and quantum size effects represent complementary geometric design strategies, with the former exploiting crystallographic anisotropy to expose intrinsically active planes, and the latter leveraging lattice distortion to create active sites through orientation-independent structural modifications.

Lattice strain effects

After the identification of active facets, artificially induced lattice strain was found to offer a non-destructive physical approach to modulate the surface electronic states. The integration of isolated Ru single atoms into Co_3O_4 via atomic substitution induces a local compressive strain that contracts the Co-O bonds, enhancing d-p orbital hybridization and increasing the covalency. This strain-fortified structure thermodynamically raises the O vacancy formation energy, enhancing the retention of lattice oxygen. This approach enabled stable OER under acidic conditions for more than 1,000 h at 10 mA cm^{-2}[66]. This strain may contribute to structural retention under the reported conditions.

In contrast, the dynamic lattice breathing concept enables adaptive resilience, in which Nd-doping and O vacancies induce local, reversible strain fluctuations in Co-O and Nd-O bonds through electric-field-driven bond-length modulation under an applied potential. This breathing mode may accommodate steric changes associated with evolving intermediates and may contribute to mechanical resilience during acidic OER [Figure 5B][67]. The comparison between the static compressive strain (Ru) and the dynamic breathing strain (Nd) highlights two divergent design philosophies: one prioritizes constant structural modification intended to reduce degradation, while the other emphasizes a real-time adaptive response to reaction transients. Both strategies have been associated with improved acidic-OER stability under the reported testing conditions. This juxtaposition suggests that the choice of strain strategy should be tailored to the dominant deactivation

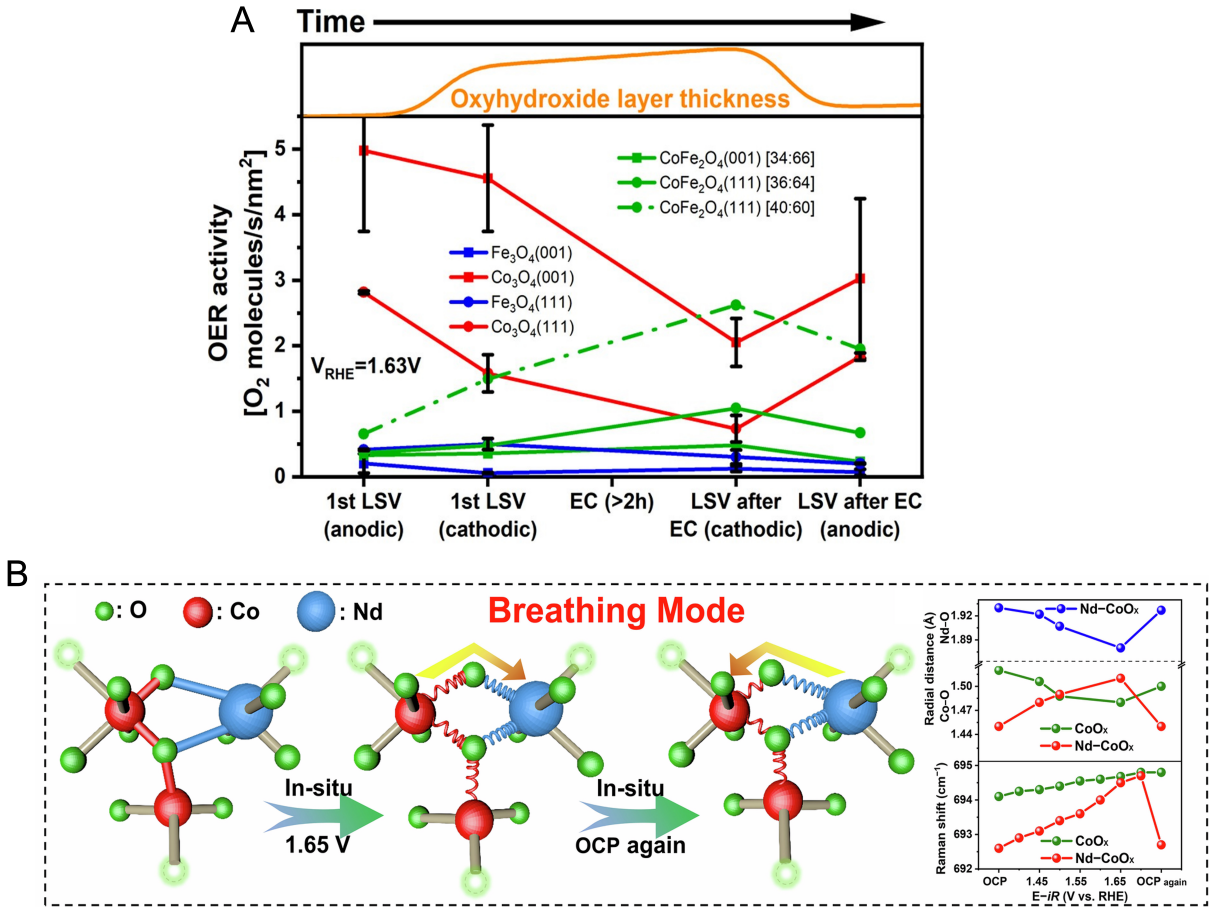


Figure 5. (A) Comparison of OER activity for epitaxial spinel oxide thin films (Co_3O_4, $CoFe_2O_4$, Fe_3O_4) with (001) and (111) facets. (A) is reproduced with permission from Ref.[64]. Licensed under CC BY 4.0; (B) Atomic structural model of the breathing mode in Nd-CoO_x and its reversible bond-length and spectroscopic responses, compared with CoO_x. (B) is reproduced with permission from Ref.[67]. Licensed under CC BY-NC-ND 4.0. OER: Oxygen evolution reaction; LSV: linear sweep voltammetry; RHE: reversible hydrogen electrode; EC: electrochemistry; OCP: open-circuit potential.

mechanism under specific operating conditions.

Operando dynamic reconstruction

For both static and dynamic strain engineering, spinels under strong anodic polarization may undergo surface reconstruction into amorphous metal (oxy)hydroxide phases, the extent and reversibility of which are composition-, facet-, electrolyte-, and potential-dependent[68-71]. The divergent behaviors of Co_2MnO_4 and $CoMn_2O_4$ vividly illustrate that the reconstruction trajectory dictates the ultimate performance, as Co_2MnO_4 transforms into a stable Co-Mn (oxy)hydroxide active phase approximately 2 nm thick, while $CoMn_2O_4$ evolves into a low-activity, Mn-rich oxide[72]. The transformation is mainly confined to the near-surface region, leaving a residual spinel framework beneath it. The initial Co/Mn stoichiometry influences the reconstructed phase, but the persistence of the original facet and strain state under OER conditions has not been established.

Capturing the active phase identity requires advanced operando techniques. Quick X-ray absorption spectroscopy combined with neural networks tracked T_d and O_h site evolution in $Co_xFe_{3-x}O_4$, revealing compositional segregation in which a Co-rich phase reversibly formed edge-sharing Co^{3+}-O_6 clusters that served as catalytically relevant centers[73]. The study indicated localized surface reorganization but did not establish a uniform reconstruction depth or complete bulk conversion; thus, the residual spinel may support

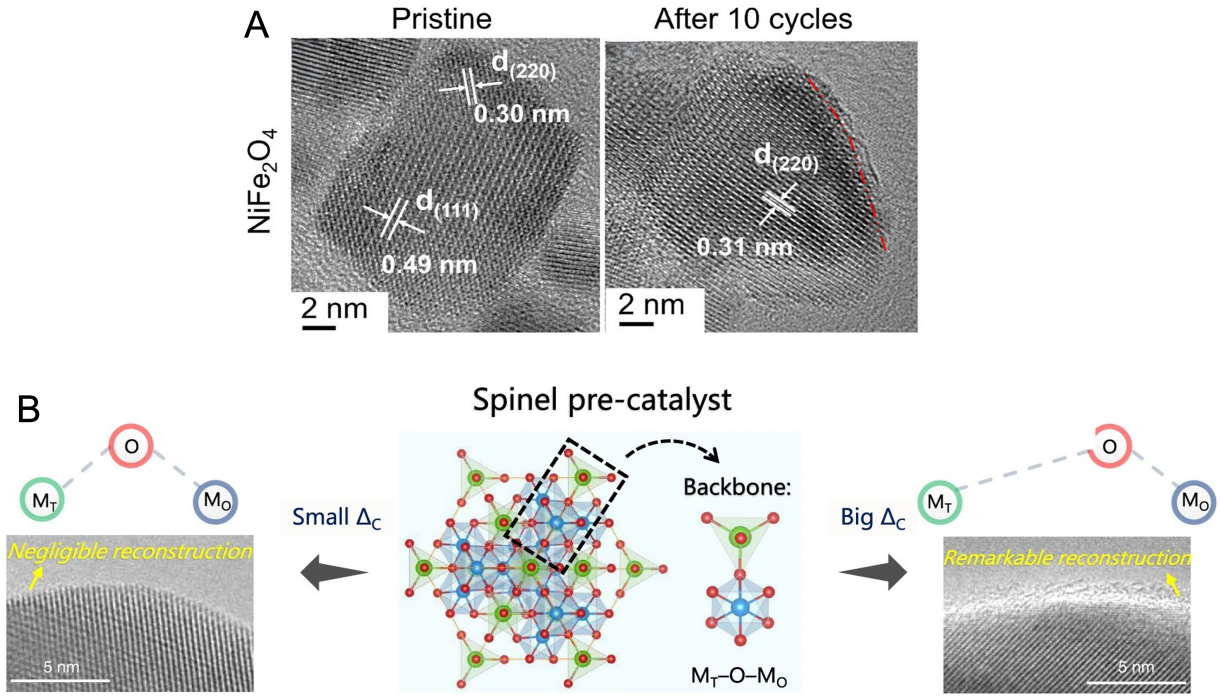


Figure 6. (A) High-resolution transmission electron microscopy (HRTEM) images of $NiFe_2O_4$ nanoparticles before and after OER cycling. (A) is reproduced with permission from Ref.[74]. Licensed under CC BY 4.0; (B) Schematic of the correlation mechanism between structure, covalency, and the degree of surface reconstruction in spinel oxides. (B) is reproduced with permission from Ref.[78]. Licensed under CC BY 4.0. OER: Oxygen evolution reaction.

the reconstructed species, while the relevance of the original facet and strain remains unresolved. Multimodal operando surface-enhanced Raman spectroscopy of $NiFe_2O_4$ showed that reconstruction was self-limited and produced an ultrathin (~1 nm) O-rich amorphous layer, as observed in high-resolution transmission electron microscopy (HRTEM) images obtained after OER cycling [Figure 6A]. This layer was associated with a Tafel slope of approximately 40 mV dec^{-1}[74]. The underlying spinel framework was largely retained, although the layer's reversibility and links to the original facet or strain were not established. Together, these studies show that reconstruction may produce discrete clusters or continuous amorphous layers, with depth, reversibility, and descriptor relevance depending on composition and operating conditions.

He *et al.* used atom-probe tomography to map Co-Cr spinels at the atomic scale and showed that vacancies induced by Cr leaching facilitated hydroxide intercalation, forming a 2-4 nm-thick, highly reversible $(Co^{II}_{Td}Co,Cr)(OH)_2 \leftrightarrow (Co^{III}_{Oct}Co,Cr)OOH$ active layer. By contrast, Co_2CrO_4 formed a self-limited layer approximately 1-2 nm thick, with Cr depletion associated with rapid deactivation[75]. The residual spinel likely supports the reconstructed layer and regulates Cr transport, while the roles of the initial Cr distribution, facet, and strain in the activated state remain incompletely established. Furthermore, directly synthesized CoOOH has been investigated as a comparison material under OER conditions. The Co(III) species in CoOOH can evolve into higher-valence Co species as the applied potential increases and may contribute to catalytic activity[76]. However, these results do not provide evidence for operando reconstruction of a spinel precursor and should not be generalized to all cobalt-based spinels[77].

The dynamic surface reconstruction of spinels is governed by the interplay between thermodynamic phase

stability and kinetic factors. Pourbaix thermodynamics determines the tendency of a given spinel composition to remain stable or transform into oxides, hydroxides, oxyhydroxides, or dissolved species at a specified pH and applied potential. Within this thermodynamic framework, intrinsic covalency polarity can serve as a useful, but not universal, descriptor of reconstruction behavior. In selected model systems, greater covalency at O_h sites than at T_d sites has been proposed to contribute to charge imbalance, lattice disruption, and surface transformation toward oxyhydroxide species [Figure 6B][78]. However, M-O covalency, defect chemistry, cation occupancy, and lattice strain also affect bond cleavage, metal dissolution, atomic redistribution, and reconstruction depth. Covalency polarity is therefore a contributing descriptor that must be considered alongside electrochemical thermodynamics and other kinetic factors, rather than treated as the sole reconstruction driver. A key design objective is to control the extent of reconstruction and achieve an appropriate active-layer depth. The electrolyte pH, the lattice stoichiometry, and heteroatom doping (Fe, Cr, W, and Mo) can be used to govern the evolution trajectory[79-85]. To prevent destructive over-reconstruction, strategies such as multi-principal element doping and inorganic-organic hybrid interfaces curb the inward penetration of the phase transition front, preserving the bulk rigidity[86,87]. Related behavior has also been reported in nanoscale confinement systems, although the generality of this trend remains to be established[88,89]. These approaches collectively represent a deliberate shift from passive observation to active phase-change management, integrating insights from covalency polarity and compositional control to steer reconstruction toward an optimal balance between activity and durability.

INTERFACIAL COUPLING AND CONFINED INTERFACES

Interfacial coupling and confined interfaces provide complementary approaches for regulating spinel-based catalysts. Interfacial coupling mainly promotes charge redistribution and electronic communication, whereas physical confinement and solid-liquid microenvironmental control regulate mass transport, active-site accessibility, and local reaction conditions. Together, these strategies may improve OER activity or durability relative to selected single-phase reference materials under comparable conditions[90,91].

Interfacial coupling and charge flow steering

Interfacial coupling occurs through the strategic construction of heterogeneous architectures, effectively combining spinels with other functional phases to modify the local electronic structure through strong interphase interactions. Central to this regulatory mechanism is the BIEF, an internal electrostatic gradient driven by a spontaneous charge redistribution that occurs during the equilibration of Fermi levels between disparate phases, necessitated by their differing work functions. By redistributing charge, the BIEF alters electron density at active sites and may optimize intermediate chemisorption and conversion energetics. This basic BIEF effect serves as a starting point for more sophisticated designs. Double-shell-structured mixed spinels (AB_2O_4) exploit cross-interface charge rearrangement in synergy with defect engineering to weaken the deprotonation energy barrier of the critical *OOH intermediate[92]. These architectures demonstrate that BIEF regulation can extend beyond simple charge-transfer enhancement to include coordinated modification of interfacial electronic structure and reaction energetics.

A more advanced strategy uses rare-earth oxides as interfacial electron pumps. Coupling CeO_2 with Co_3O_4 leverages the abundant oxygen vacancies and 4f states of CeO2 to promote directional electron transfer, shifting the Co d-band center upward to balance intermediate adsorption [Figure 7A][93]. This electron pump effect is distinct from simple BIEFs because the redox-active nature of CeO_2 (Ce^{4+}/Ce^{3+}), coupled with O-vacancy-mediated dynamics, provides a dynamic electron reservoir that can respond to changes in the reaction environment[94]. In acidic conditions, a $Co_2MnO_x@Co_3O_4$ heterostructure was also shown to induce a d-band center upshift; the primary benefit, however, was the formation of corrosion-resistant high-valence species that extended the lifetime of Co_3O_4 from 12 to over 370 h[95]. Ag nanoparticles anchored on spinel

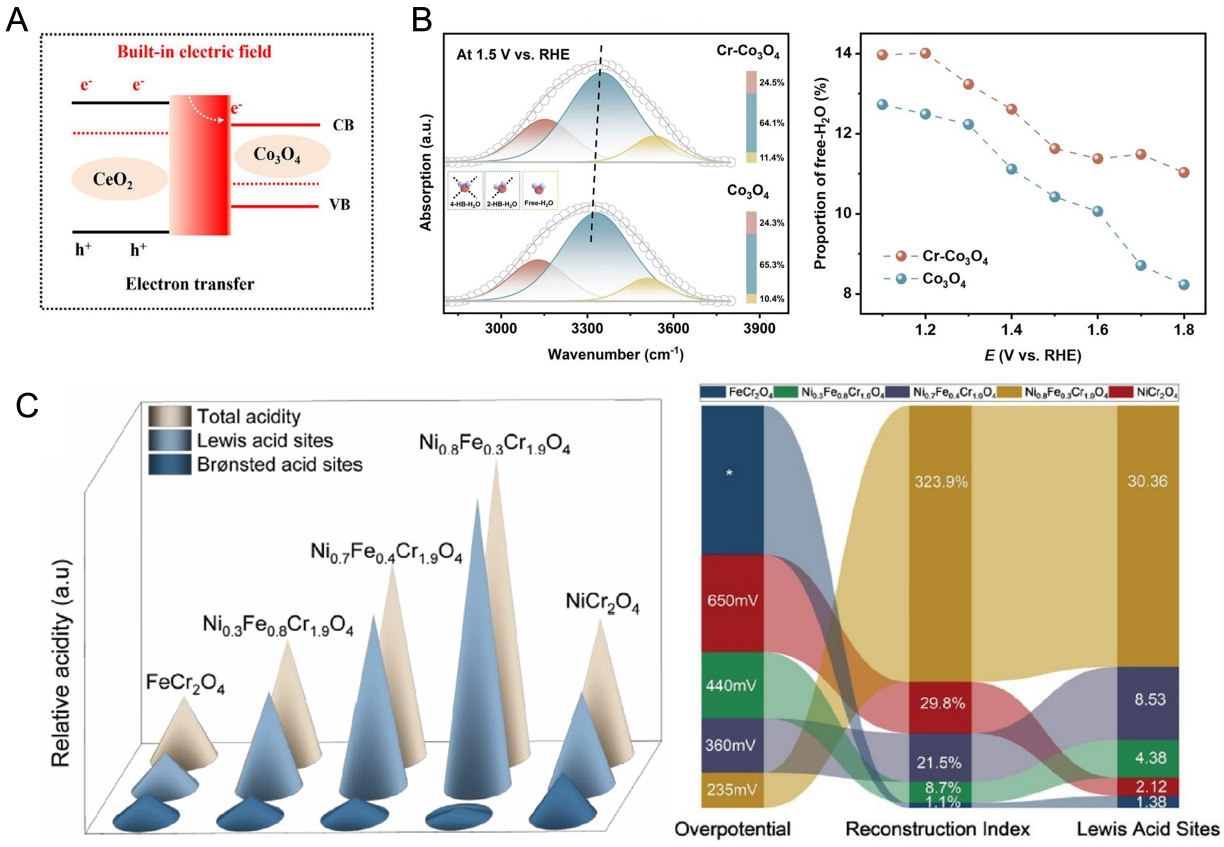


Figure 7. (A) Schematic illustration of BIEF-driven electron transfer at the CeO_2/Co_3O_4 heterojunction interface. (A) is reproduced with permission from Ref.[93]. Copyright 2025, Wiley-VCH GmbH; (B) Operando infrared spectra of interfacial water on Cr-Co_3O_4 and pristine Co_3O_4 surfaces, alongside the calculated proportions of free water across various applied potentials. (B) is reproduced with permission from Ref.[109]. Licensed under CC BY-NC-ND 4.0; (C) Correlation analysis of Lewis acid site density, reconstruction index, and OER overpotential for chromite spinel catalysts with varying Ni/Fe compositions, revealing the pivotal role of Lewis acidity in governing surface reconstruction and oxygen evolution activity. (C) is reproduced with permission from Ref.[110]. Copyright 2025, Wiley-VCH GmbH. CB: Conduction band; VB: valence band; RHE: reversible hydrogen electrode; BIEF: built-in electric field.

supports similarly optimized the adsorption of adjacent Co T_d sites[96]. These examples show that while both CeO_2 coupling and surface MnO_x coating strategies can achieve electronic restructuring of the spinel/oxide interface, the former operates as a dynamic electron reservoir to balance intermediate adsorption, whereas the latter suppresses metal dissolution by forming a corrosion-resistant overlayer in acidic media.

Physical confinement strategies and mass transfer microenvironment remodeling

Physical confinement focuses on establishing protective spatial boundaries or constructing micro-/nano-void structures to confine active sites within defined regions. This confinement provides physical shielding to prevent the aggregation or leaching of active sites during reactions and may alter local reactant concentrations through confinement effects. These cavities contain tailored diffusion pathways that can alter interfacial mass transport. Physical confinement strategies reshape the reaction microenvironment at multiple length scales to enhance mass transfer and stabilize active sites[97].

Biomimetic structures with superhydrophilicity and superaerophobicity further allow catalytically generated bubbles to detach instantaneously, ensuring efficient exchange of reactants and products. These macroporous scaffolds primarily address gas-liquid diffusion limitations. As confinement is reduced to the nanoscale, high-curvature closed cavities such as yolk-shell nanocages or onion-like carbon interiors provide dual functionality[98,99]. They physically shield metal sites from corrosive electrolytes while inducing d-π

orbital hybridization and localized tip effects to accelerate electron transport[100]. At the atomistic limit, mesoporous single-crystalline matrices anchor single atoms at the pore edges, creating abundant active edge sites, while the single-crystalline structure substantially reduces metal leaching. For example, Ir single atoms anchored at ~20 nm pore edges in single-crystalline Co_3O_4 reduced leaching to approximately 20%-25% of the original level under acidic conditions[101]. Similarly, edge-specific confinement of Co_3O_4 nanoclusters on ReS_2 facets established Re-O-Co bridges that drove a spin-state transition in Co^{3+} that optimized intermediate adsorption; this study is used only as a transferable confinement/interface concept and not as direct OER evidence[102]. These edge-confined systems illustrate the coupled effects of confinement geometry and electronic regulation on catalytic properties. Thus, the progression from mesoporous networks to atomic-level edge confinement has followed a path of continuously increasing precision in controlling both the physical and electronic microenvironment.

Regulation of solid-liquid interface microenvironment

Solid-liquid microenvironment control involves the regulation of local pH gradients, ion speciation, and water molecular organization at the catalyst-electrolyte interface. This strategy transcends traditional solid-state structural design by employing functionalization to regulate the proportion of free water or generate localized alkaline layers that repel interfering ions. The microenvironment also includes intermediate species coverage, which can be regulated through functional interfacial engineering[103-105]. In seawater electrolysis, chloride-induced corrosion can be suppressed by generating a local alkaline environment[106]. For example, a Cr_2O_3-modified Co-based spinel promoted water dissociation, producing a local OH^--enriched layer that electrostatically repelled Cl^-, enabling stable operation at 1.0 A cm^{-2} for over 100 h[107].

Endogenous protection represents a self-sustaining strategy where the protective layer is autonomously generated from the electrode material itself. Mo-doped high-entropy $(CrFeMnNiCoMo)_3O_4$ formed surface Mo-rich species that repelled Cl^- via electrostatic and physical blocking, while $(CrMnFeCoNi)_3O_4$ formed a Cr_2O_3 passivation layer *in situ*. The severe lattice distortion inherent to these high-entropy spinels also altered active-site spacing, sterically hindering Cl-M bond formation. Together, OH^- selectivity and physical blocking contributed to stable operation for 1,000 h at 200 mA cm^{-2}[108]. These approaches share a common principle of local alkalinity and anion repulsion, although the implementation can be exogenous (surface coating) or endogenous (self-generated by the spinel itself), with the latter offering the advantage of dynamic self-renewal.

The interfacial water network profoundly impacts the OER kinetics, and its modulation is emerging as a critical design axis. Dynamic Cr doping of Co_3O_4 at T_d sites increased the surface coverage of Cr^{3+}-OH species, which weakened the interfacial hydrogen-bond network and shifted water from a rigid, coordinated state to more reactive free water, as evidenced by *in situ* attenuated total reflection surface-enhanced infrared absorption spectroscopy. This optimized interfacial environment facilitated water dissociation and lowered the kinetic barrier, which enabled operation at 1 A cm^{-2} with durability exceeding 750 h in a PEMWE [Figure 7B][109]. In parallel, the Lewis acidity of the spinel surface has been correlated with the extent of reconstruction into active phases. In chromite spinels, tuning the Ni/Fe ratio directly modulated the Lewis acid site density, and $Ni_{0.8}Fe_{0.3}Cr_{1.9}O_4$, with the highest Lewis acidity, underwent the most extensive surface reconstruction and delivered an overpotential of only 235 mV [Figure 7C][110]. These two findings suggest a possible relationship, as Lewis acid sites can polarize and activate interfacial water molecules, an effect that may resemble the influence of Cr doping on the hydrogen-bond network. Both effects may facilitate the formation of catalytically relevant oxyhydroxide species under the reported conditions. This intrinsic connection between the surface acidity, interfacial water structure, and phase reconstruction provides a possible framework for the microenvironmental engineering of spinel-based OER catalysts.

The adsorption of key intermediates such as *OH can be intentionally manipulated in opposite directions depending on the catalyst's intrinsic stability. Atomically dispersed Ru on Co_3O_4 lowered the *OH coverage on adjacent Co sites to prevent over-accumulation of oxidative species and metal dissolution, thus preserving structural stability[111]. In contrast, incorporating a high density of W single atoms into Co_3O_4 enhanced OH^- adsorption and was associated with reconstruction into active oxyhydroxide species[112]. This dichotomy demonstrates that the optimal *OH binding is context-dependent: weakening *OH adsorption can preserve stability when the spinel is prone to over-oxidation, whereas strengthening adsorption may promote surface transformation when the spinel is too inert. Finally, microenvironment remodeling can exploit the dynamic feedback of *in situ* generated species. SO_4^{2-} ions leached during the initial reaction stages of an Ni-Co spinel were readsorbed onto the surface, optimizing intermediate binding and stabilizing O vacancies for prolonged operation at current densities in the ampere range[113]. This self-optimizing behavior integrates confinement, adsorption, and defect stabilization into a dynamic microenvironment-control process in which the catalyst may adapt its surface chemistry during operation.

PERFORMANCE EVALUATION UNDER REPORTED CONDITIONS

Water-electrolysis devices are moving toward deployment at the megawatt and gigawatt scales, posing increasingly stringent demands on the cost-effectiveness, large-scale reproducibility, and realistic durability of electrocatalysts. This review summarizes condition-specific performance data for multiscale site-engineering strategies using representative spinel catalysts tested in different systems. It must be emphasized that, because of substantial variation in electrolyte pH, catalyst loading, iR-drop compensation methods, and test temperature (e.g., 25 °C *vs.* 80 °C) across studies, direct cross-literature comparisons of overpotential values can be misleading. The performance summary presented herein is intended to illustrate the performance reported for each strategy under specific experimental protocols, rather than to provide an absolute ranking. One aspect of the evaluation framework summarizes electrochemical metrics obtained in three-electrode measurements. The listed overpotentials and Tafel slopes are reported together with the available testing conditions and measurement basis to describe the reported electrochemical behavior; they are not treated as direct measures of intrinsic kinetics solely because they were obtained in a three-electrode configuration. Because the normalization procedures and experimental conditions are not uniform across the cited studies, the entries are presented descriptively and are not used for cross-study ranking [Table 2]. A second aspect considers the reported device-level relevance of spinel-based catalysts by summarizing reported performance from full-cell devices and selected liquid-electrolyte tests, including PEMWE and anion-exchange-membrane water electrolyzers (AEMWE). Available information on electrolyzer configuration, electrolyte or feed, catalyst loading, operating conditions, current density, cell voltage, stability, and selectivity is summarized [Table 3]. Because device architectures and operating protocols are not uniform, these results are presented as representative, non-ranked examples rather than as a direct industrial benchmark. Further validation under standardized cell configurations, realistic operating conditions, and extended durability tests remains necessary to assess practical electrolyzer deployment.

Realizing the technological potential of site-engineered spinel catalysts will also require closing the gap between laboratory-scale durability testing, which typically lasts tens to hundreds of hours, and the lifetimes of thousands of hours demanded by industrial electrolyzers. Scale-up barriers, such as achieving reproducible large-batch synthesis, applying uniform electrode coatings, and maintaining site-engineering precision beyond gram-scale production, must also be overcome. Addressing these gaps will be essential for translating the mechanistic insights discussed in this review into technologically relevant catalyst systems.

Table 2. Condition-specific three-electrode OER performance data for representative spinel-based catalysts

Material	Cation-site or structural feature	Electrolyte	Loading and substrate	*iR*-drop compensation	Temperature	Overpotential	Tafel slope	Electrochemically active surface area (ECSA) or mass-normalized activity	Faradaic efficiency	Stability and dissolution	Reconstructed phase	Mechanistic evidence	Ref.
$(FeCoNiCrMn)_3O_4$	High-entropy spinel with multication disorder	Purified Fe-free 1.0 M KOH	Approximately 0.204 mg cm^{-2} on a glassy carbon disk for activity tests; carbon cloth used for stability tests	80% *iR* compensation applied	Room temperature	239 mV at 10 mA cm^{-2}	52.4 mV dec^{-1}	Not reported	Not reported	24 h at 100 mA cm^{-2}; quantitative dissolution not reported	High-valence surface species; exact phase not clearly identified	High-entropy structure and surface evolution; pathway assignment not directly established	[36]
$ZnFe_2O_4$	Zn vacancies	1.0 M KOH	0.874 mg cm^{-2}, nickel foam	*iR* compensation applied to linear sweep voltammetry (LSV) curves; correction level not reported	Room temperature	236 mV at 10 mA cm^{-2}	67.24 mV dec^{-1}	Not reported	Not reported	50 mA cm^{-2} for 22.5 h; Zn reached approximately 0.08 mg L^{-1} and Fe leaching was minimal	$ZnFe_2O_4$ spinel structure retained; no distinct reconstructed phase identified	O 2p-band upshift and electrochemical data support enhanced lattice-oxygen participation; indirect evidence for LOM	[48]
$NiFe_2O_4$	Ni^{4+} centers and Ni vacancies	Purified Fe-free 1.0 M KOH	1 mg cm^{-2} on acid-treated carbon cloth	*iR* compensation applied to LSV curves; correction level not reported	Not reported	293 mV at 500 mA cm^{-2}	43.8 mV dec^{-1}	Not reported	Not reported	Chronopotentiometry at 100 mA cm^{-2} for 50 h; dissolution not reported	Partial reconstruction to amorphous NiFeOOH; $NiFe_2O_4$ phase retained	Enhanced M-O covalency; specific pathway assignment not established	[51]
$Co_{2.5}Ga_{0.5}O_4$	Ga-substituted spinel; octahedral-site assignment	1.0 M KOH	Approximately 1.6 mg of total catalyst was loaded onto a ~ 0.25 cm^2 carbon-paper electrode	*iR* compensation applied to LSV curves; correction level not reported	Room temperature	220 mV at 10 mA cm^{-2}	56 mV dec^{-1}	ECSA-normalized LSV curves reported; numerical activity value not provided	Not reported	Not reported	Not reported; post-OER reconstructed phase was not characterized	AEM supported by DFT calculations; no direct operando pathway evidence reported	[55]
$Ni_{0.8}Fe_{0.3}Cr_{1.9}O_4$	Lewis-acid-rich chromite spinel	1.0 M KOH	A 4 mg catalyst sample was dispersed in a water/ethanol/Nafion ink and drop-cast onto a 3 mm glassy carbon electrode; the areal loading was not reported	90% *iR* compensation applied	Not reported	235 mV at 10 mA cm^{-2} after 500 cyclic voltammetry (CV) cycles	70 mV dec^{-1} after 50 CV cycles; activated value not reported	ECSA-normalized activity reported; numerical value not provided	Not reported	500 CV cycles; 40 h at the potential required for 10 mA cm^{-2}, with > 60% current retention; dissolution not reported	Oxyhydroxide-rich surface overlayer formed after electrochemical activation; underlying spinel framework retained	Lewis-acid-site regulation and reconstruction correlation; direct pathway assignment not established	[110]

OER: Oxygen evolution reaction; LOM: lattice oxygen mechanism; LSV: linear sweep voltammetry; AEM: adsorbate evolution mechanism; DFT: density functional theory; *iR*: ohmic drop.

Table 3. Condition-specific performance of full-cell PEMWEs and AEMWEs

Active material	Electrolyzer type and configuration	Membrane and cell information	Electrolyte or feed	Catalyst loading and electrode information	Temperature and pressure	Current density and voltage	Stability and degradation	Faradaic efficiency, crossover, and selectivity	Unique advantages or mechanisms	Ref.
La/Mn-doped Co_3O_4 nanofibers (LMCF)	PEMWE, membrane-electrode assembly (MEA)	Nafion 115; active area = 5 cm^2	Preheated deionized water fed to the anode at 10 mL min^{-1}	LMCF anode: 2.0 mg cm^{-2}; Pt cathode: 0.4 mg cm^{-2}	60 °C for the reported PEMWE polarization and galvanostatic measurements; atmospheric pressure	2.0 A cm^{-2} at 2.47 V without *iR* compensation	Over 100 h at 210 mA cm^{-2}; 10,000-cycle accelerated stress test between 1.4 and 1.7 V at 300 mV s^{-1} with 10 s dwell at each voltage	Not reported	La/Mn doping improves conductivity and surface stability	[25]
Cr-doped Co_3O_4	PEMWE, MEA	Nafion 212 membrane; active area = 5 cm^2; porous transport layer not reported	Pure water fed to the anode; flow rate not reported	CoCr anode loading: 4.8 mg cm^{-2}; Pt/C cathode loading: 0.3 mg cm^{-2}	Durability test: 80 °C; pressure not reported. Temperature for the reported polarization value not specified	1.5 A cm^{-2} at 2.17 V; *iR* compensation status not reported	100 h at 500 mA cm^{-2} and nearly 500 h at 100 mA cm^{-2}; degradation rate not reported	Not reported	Dynamic Cr dopant promotes interfacial water activation and stabilizes Co-O bonding	[54]
Nd-CoO_x	PEMWE, MEA	Nafion 117 membrane; effective area: approximately 1.0 cm^2; porous transport layer not reported	Pure water; flow rate not reported	Nd-CoO_x anode loading: approximately 5 mg of catalyst cm^{-2}; catalyst-layer details not reported	Polarization and durability tests: 80 °C; pressure not reported	1 A cm^{-2} at 1.93 V and 2 A cm^{-2} at 2.12 V (cell voltage with 90% *iR* compensation applied)	Over 100 h at 200 mA cm^{-2} and 1.69 V; degradation rate not reported	Not reported	Oxygen vacancies promote activity; Nd-induced breathing mode provides adaptive structural stability	[67]
$(CrMnFeCoNi)_3O_4$	AEMWE, MEA	Sustainion X37-50 Grade T anion-exchange membrane; active area: 2 × 2 cm^2; porous transport layer and detailed cell geometry not reported	1 M KOH or 1 M KOH plus pretreated seawater from Kaohsiung Harbor, Taiwan	Anode loading: 2.0 mg cm^{-2}; 15 wt% ionomer; cathode loading not reported	Polarization and durability tests: 60 °C; pressure not reported	1 A cm^{-2} at 1.88 V without *iR* compensation; energy-conversion efficiency 83.8-75.8% in KOH and 84.2-73.8% in KOH + seawater	520 h at 0.5 A cm^{-2}; voltage decay was 0.33 mV h^{-1} in KOH and 0.44 mV h^{-1} in KOH containing seawater	Hydrogen Faradaic efficiency > 98.5%; quantification method not reported; crossover not reported; hypochlorite assessed by ultraviolet-visible starch-iodide colorimetry after long-term operation, with a weak 349 nm signal; detection limit not reported	High-entropy lattice stabilization and chlorine-corrosion resistance	[108]
Cr-Co_3O_4	PEMWE, MEA	Pt/C cathode; Nafion 115 membrane; active area 1 cm^2; porous transport layer not reported	Pure water circulated at 40 mL min^{-1}	Cr-Co_3O_4 anode loading: 4 mg cm^{-2}; Pt/C cathode loading: 3 mg cm^{-2}	Polarization and durability tests: 60 °C; pressure not reported	1 A cm^{-2} at 2.11 V without *iR* compensation	750 h at 1 A cm^{-2}; degradation rate not reported	Not reported	Dynamic Cr doping promotes interfacial water activation and stabilizes the Co-based spinel under acidic OER	[109]

OER: Oxygen evolution reaction; PEMWEs: proton exchange membrane water electrolyzers; AEMWEs: anion exchange membrane water electrolyzers; *iR*: ohmic drop.

CONCLUSIONS AND OUTLOOK

Summary

This review has organized and critically discussed recent advances in AB_2O_4 spinel oxides for the OER, highlighting a multi-scale framework of site-engineering strategies that have progressed from bulk regulation, through intrinsic structural dynamics, to interfacial coupling and confined interfaces. The development paradigm has transitioned from compositional trial-and-error to rational design based on fundamental physical insights, with covalency and its competitive interactions emerging as recurring descriptors across the selected examples. At the bulk level, precise control over the spin states, bond competition, high-entropy effects, and vacancy-induced changes in covalency may alter the relative contribution of AEM, LOM, or OPM under selected conditions, while theoretical descriptors such as the covalency index and center-environment features now guide the search for the optimal activity-stability balance. At the interfacial level, BIEFs arising from interfacial coupling can facilitate charge transfer, while genuine confinement strategies, including physical nanoconfinement and molecular-level microenvironmental control, can regulate mass transport and intermediate adsorption, potentially improving interfacial catalytic performance under selected conditions. Across all scales, the analyzed examples have revealed a consistent progression from single-variable tuning to multi-dimensional synergistic design, providing a structured design framework for next-generation electrocatalyst development.

Future challenges and outlook: from atomic-level microenvironment engineering to electrolyzer-system evaluation

To further evaluate the prospects of spinel-based electrocatalytic materials for electrolyzer applications, future research should focus on the following frontiers.

(1) The microscopic mechanism of interfacial water regulation should be elucidated. Traditional site engineering often focuses on the solid catalyst, while the arrangement of interfacial water molecules has been largely overlooked. Future research should utilize *in situ* spectroscopy to reveal the orientation and hydrogen-bond network of interfacial water under applied biases and their impact on proton transfer. Strategies should be developed to manipulate the solvation sheath by introducing hydrophobic functional groups or modulating local charges to accelerate the reaction kinetics.

(2) The activity-stability trade-off remains a major challenge. Because lattice-oxygen participation can be associated with structural instability in some systems, future research in site engineering should aim to develop dynamically stable systems. This includes incorporating high-entropy components to anchor the bulk skeleton and utilizing self-healing mechanisms to dynamically compensate for lost lattice O, with the aim of improving stability under acidic or high-current conditions while retaining catalytic activity.

(3) Multiscale *in situ* characterization and multimodal, data-driven approaches should be advanced. Synchrotron-based techniques and *in situ* transmission electron microscopy should be employed to track the atomic-level evolution of active sites.

(4) Research should advance system integration for industrial applications. Future research should account for the requirements of application-relevant PEMWE or AEMWE. This demands catalysts with high current densities, excellent electrical conductivities, strong adhesion to the electrode support, and resistance to impurity-ion poisoning, bridging the gap between laboratory evaluation and full-cell device operation.

Beyond catalytic performance, the practical deployment of site-engineered spinel catalysts also depends on several factors: the scarcity of Co and Ni and the cost and scarcity of Ru, Ir, Bi, and rare-earth dopants; the synthesis complexity and phase reproducibility associated with precise site-selective doping; catalyst-support adhesion under long-term operation; and end-of-life recovery of critical and precious elements. These considerations, while beyond the catalytic scope of this review, identify important research priorities for bridging site engineering with sustainable, large-scale implementation.

DECLARATIONS

Authors' contributions

Writing - original draft preparation: Yang, B.
Writing - review & editing, conceptualization: Zhu, E.; Yang, B.
Validation: Jia, H.
Data curation: Wang, Y.
Visualization: Zhu, E.
Project administration: Liu, Z. Q.
Funding acquisition: Lei, B. X.; Zhu, E.

Availability of data and materials

Not applicable.

Statement on AI and AI-assisted tools

During the preparation of this manuscript, the AI tool Gemini 3 Pro Image (model ID gemini-3-pro-image-preview, released 2025-11-20) was used to assist in creating the crystal structure shown in Figure 2, and DeepSeek (version V3.2, DeepSeek AI, released 2025-12-01) was used for language editing. These tools did not influence the study design, data collection, analysis, interpretation, or the scientific content of the work. All authors take full responsibility for the accuracy, integrity, and final content of the manuscript.

Financial support and sponsorship

This work was supported by the National Natural Science Foundation of China (No. 22362006, 22278094 and U24A20541), the Natural Science Foundation of Guangxi Province (No. 2023GXNSFAA026444, 2026GXNSFBA00640151), the Guangxi Young Elite Scientist Sponsorship Program (No. GXYESS2025082), and the Guangxi Minzu University Research Funding Project (No. 2022KJQD36, 2022MDKJ005).

Conflicts of interest

All authors declared that there are no conflicts of interest.

Ethical approval and consent to participate

Not applicable.

Consent for publication

Not applicable.

Copyright

© The Author(s) 2026.

Supplementary Materials

Supplementary Materials

REFERENCES

1. Kottaichamy, A. R.; Volokh, M.; Tzadikov, J.; Shalom, M. Efficient and scalable electrochemical energy systems via peroxide-mediated redox chemistry. *Adv. Sci.* **2026**, *13*, e17218. DOI PubMed PMC
2. Hu, Z.; Wu, H.; Yong, X.; et al. Advances in dual-site mechanisms for designing high-performance oxygen evolution electrocatalysts. *eScience* **2025**, *5*, 100403. DOI
3. Rong, C.; Sun, Q.; Zhu, J.; et al. Advances in stabilizing spinel cobalt oxide-based catalysts for acidic oxygen evolution reaction. *Adv. Sci.* **2025**, *12*, e09415. DOI
4. Jiang, Y.; Zheng, Y.; Qiao, S. An effective strategy to boost lattice-oxygen-mediated acidic oxygen evolution. *Chem* **2023**, *9*, 1628-30. DOI
5. Rong, C.; Huang, X.; Arandiyan, H.; Shao, Z.; Wang, Y.; Chen, Y. Advances in oxygen evolution reaction electrocatalysts via direct oxygen-oxygen radical coupling pathway. *Adv. Mater.* **2025**, *37*, e2416362. DOI
6. Xiao, K.; Liu, Z. Regulation strategy of spinel OER electrocatalyst. *Chin. Sci. Bull.* **2025**, *70*, 2966-80. DOI
7. Hao, X.; Wang, R.; Tan, X.; et al. Fabricating spinel-type high-entropy oxides of $(Co, Fe, Mn, Ni, Cr)_3O_4$ for efficient oxygen evolution reaction. *Materials* **2024**, *17*, 3415. DOI PubMed PMC
8. Liu, Y.; Ma, C.; Zhang, Q.; et al. 2D electron gas and oxygen vacancy induced high oxygen evolution performances for advanced Co_3O_4/CeO_2 nanohybrids. *Adv. Mater.* **2019**, *31*, e1900062. DOI
9. Jiang, K.; Bai, H.; Zheng, W.; et al. Dynamic construction of amorphous-crystalline RuO_2-Co_3O_4 heterointerfaces enables interfacial oxide paths for acidic water oxidation. *Nano. Energy.* **2026**, *159*, 112416. DOI
10. Sarkar, A.; Wang, Q.; Schiele, A.; et al. High-entropy oxides: fundamental aspects and electrochemical properties. *Adv. Mater.* **2019**, *31*, e1806236. DOI
11. Johnstone, G. H. J.; González-Rivas, M. U.; Taddei, K. M.; et al. Entropy engineering and tunable magnetic order in the spinel high-entropy oxide. *J. Am. Chem. Soc.* **2022**, *144*, 20590-600. DOI
12. Li, Z.; Alrashood, J. S.; Manjunatha, S.; et al. High-entropy-driven electronic structure engineering in Mg-Zn-Fe-Cr spinel ferrites for multifunctional energy catalysis. *Ceram. Int.* **2026**, *52*, 42063-80. DOI
13. Zhang, T.; Liu, Y.; Tong, L.; et al. Oxidation state engineering in octahedral Ni by anchored sulfate to boost intrinsic oxygen evolution activity. *ACS. Nano.* **2023**, *17*, 6770-80. DOI
14. Zhang, L.; Xu, Q.; Xia, L.; et al. Asymmetrically tailored catalysts towards electrochemical energy conversion with non-precious materials. *Chem. Soc. Rev.* **2025**, *54*, 5108-45. DOI
15. Yuan, C.; Huang, S.; Zhao, H.; et al. Vacancy defect tuning of electronic structures of transition metal (hydr)oxide-based electrocatalysts for enhanced oxygen evolution. *Energy. Adv.* **2023**, *2*, 73-85. DOI
16. Karthikeyan, S. C.; Ramakrishnan, S.; Prabhakaran, S.; et al. Low-cost self-reconstructed high entropy oxide as an ultra-durable OER electrocatalyst for anion exchange membrane water electrolyzer. *Small* **2024**, *20*, e2402241. DOI
17. Li, X.; Kou, Z.; Dai, J.; Sun, H.; Wang, J.; Zheng, S. Advances in spinel-type electrocatalysts: leveraging ligand field theory to elucidate structure-property relationships. *J. Materiomics.* **2025**, *11*, 101031. DOI
18. Chen, M.; Kitiphatpiboon, N.; Feng, C.; Abudula, A.; Ma, Y.; Guan, G. Recent progress in transition-metal-oxide-based electrocatalysts for the oxygen evolution reaction in natural seawater splitting: a critical review. *eScience* **2023**, *3*, 100111. DOI
19. Ma, S.; Cao, Z.; Zhao, Y.; et al. Tetrahedral-site doping modulation in Mn_3O_4 toward improved water oxidation activity and stability. *Chem. Eng. J.* **2026**, *537*, 176550. DOI
20. Rafique, M.; Yao, T.; Ma, S.; et al. High-entropy engineering of cobalt spinel oxide breaks the activity-stability trade-off in oxygen evolution reaction. *Adv. Funct. Mater.* **2026**, *36*, e12495. DOI
21. Ye, Y.; Xu, J.; Li, X.; et al. Orbital occupancy modulation to optimize intermediate absorption for efficient electrocatalysts in water electrolysis and zinc-ethanol-air battery. *Adv. Mater.* **2024**, *36*, e2312618. DOI
22. Xing, G.; Lu, M.; Zhang, G.; et al. Spin-state engineering via Cr^{3+} incorporation in Co_3O_4 spinel for efficient bifunctional oxygen electrocatalysis. *Carbon. Energy.* **2026**, *8*, e70161. DOI
23. Pan, S.; Li, H.; Wang, T.; et al. Er-doping enhances the oxygen evolution performance of cobalt oxide in acidic medium. *ACS. Catal.* **2024**, *14*, 13814-24. DOI
24. Zhang, Z.; Zhu, J.; Shi, B.; et al. Modulating the electronic structures of Co-based spinel compounds via rare earth tetrad effect. *J. Am. Chem. Soc.* **2026**, *148*, 4450-61. DOI
25. Chong, L.; Gao, G.; Wen, J.; et al. La- and Mn-doped cobalt spinel oxygen evolution catalyst for proton exchange membrane electrolysis. *Science* **2023**, *380*, 609-16. DOI
26. Wang, Z.; Huang, J.; Wang, L.; et al. Cation-tuning induced d-band center modulation on Co-based spinel oxide for oxygen reduction/evolution reaction. *Angew. Chem. Int. Ed.* **2022**, *61*, e202114696. DOI

27. Zhou, Y.; Sun, S.; Wei, C.; et al. Significance of engineering the octahedral units to promote the oxygen evolution reaction of spinel oxides. *Adv. Mater.* **2019**, *31*, e1902509. DOI
28. Wang, Z.; Wu, P.; Zou, X.; et al. Optimizing the oxygen-catalytic performance of Zn-Mn-Co spinel by regulating the bond competition at octahedral sites. *Adv. Funct. Mater.* **2023**, *33*, 2214275. DOI
29. Park, S.; Jang, T.; Choi, S.; et al. Iridium-cooperated, symmetry-broken manganese oxide nanocatalyst for water oxidation. *J. Am. Chem. Soc.* **2023**, *145*, 26632-44. DOI
30. Cai, M.; Cai, G.; Liu, K.; Wang, D.; Zhao, H.; He, P. Ultralow Ru loading on spinel oxide enhances oxygen coupling for efficient acidic water oxidation. *J. Am. Chem. Soc.* **2025**, *147*, 39953-63. DOI
31. Shim, J.; Ahn, H.; Kwon, H. J.; et al. Corrosion-inspired stabilization of cobalt oxide catalysts via platinum-mediated redox buffering for proton exchange membrane water electrolysis. *Adv. Mater.* **2026**, *38*, e22703. DOI
32. Lv, Y. H.; Wei, S.; Yi, S. S.; et al. Tuning octahedron sites of CoV_2O_4 via cationic competition for efficient oxygen evolution reaction. *Small* **2024**, *20*, e2402402. DOI
33. Liu, C. P.; Vang, E. H.; Priamushko, T.; Roiron, C.; Cherevko, S.; Atanassov, P. Acidic oxygen evolution reaction activity, stability, and durability of copper and/or manganese cobalt oxide spinels. *ACS. Catal.* **2025**, *15*, 7956-65. DOI PubMed PMC
34. Triolo, C.; Moulaee, K.; Ponti, A.; et al. Spinel-structured high-entropy oxide nanofibers as electrocatalysts for oxygen evolution in alkaline solution: effect of metal combination and calcination temperature. *Adv. Funct. Mater.* **2024**, *34*, 2306375. DOI
35. Zander, J.; Wölfel, J. P.; Weiss, M.; et al. Medium- and high-entropy spinel ferrite nanoparticles via low-temperature synthesis for the oxygen evolution reaction. *Adv. Funct. Mater.* **2024**, *34*, 2310179. DOI
36. Feng, B.; Chen, J.; Yang, Y.; et al. Facile synthesis of nanosized spinel high entropy oxide $(FeCoNiCrMn)_3O_4$ for efficient oxygen evolution reaction. *J. Materiomics.* **2024**, *10*, 919-27. DOI
37. Yue, X.; Qin, X.; Chen, Y.; et al. Constructing active sites from atomic-scale geometrical engineering in spinel oxide solid solutions for efficient and robust oxygen evolution reaction electrocatalysts. *Adv. Sci.* **2021**, *8*, e2101653. DOI
38. Baek, J.; Hossain, M. D.; Mukherjee, P.; et al. Synergistic effects of mixing and strain in high entropy spinel oxides for oxygen evolution reaction. *Nat. Commun.* **2023**, *14*, 5936. DOI PubMed PMC
39. Fan, J.; Xiang, X.; Liu, Y.; et al. Defect-rich high-entropy spinel oxide as an efficient and robust oxygen evolution catalyst for seawater electrolysis. *SusMat* **2025**, *5*, e70010. DOI
40. Li, Y.; Zhang, Z.; Li, C.; et al. Introducing phosphorus into spinel nickel ferrite to enhance lattice oxygen participation towards water oxidation electrocatalysis. *Appl. Catal. B. Environ. Energy.* **2024**, *355*, 124116. DOI
41. Fu, Q.; Wong, L. W.; Zheng, X.; et al. The role of oxygen vacancies: triggering lattice oxygen oxidation mechanism in acidic OER. *Nano. Energy.* **2026**, *149*, 111731. DOI
42. Liu, Z.; Kong, Z.; Cui, S.; et al. Electrocatalytic mechanism of defect in spinels for water and organics oxidation. *Small* **2023**, *19*, e2302216. DOI
43. Ma, Y.; Li, K.; Xue, Z.; et al. Modulating the reaction pathway of tricobalt tetraoxide-based catalysts for advanced oxygen evolution. *Nano. Res.* **2026**, *19*, 94908434. DOI
44. Sun, L.; Feng, M.; Peng, Y.; et al. Constructing oxygen vacancies by doping Mo into spinel Co_3O_4 to trigger a fast oxide path mechanism for acidic oxygen evolution reaction. *J. Mater. Chem. A.* **2024**, *12*, 8796-804. DOI
45. Deng, Q.; Li, H.; Pei, K.; et al. Strategic design for high-efficiency oxygen evolution reaction (OER) catalysts by triggering lattice oxygen oxidation in cobalt spinel oxides. *ACS. Nano.* **2024**, *18*, 33718-28. DOI
46. Ren, X.; Zhai, Y.; Yang, N.; Wang, B.; Liu, S. Lattice oxygen redox mechanisms in the alkaline oxygen evolution reaction. *Adv. Funct. Mater.* **2024**, *34*, 2401610. DOI
47. Guo, P.; Shi, L.; Liu, D.; et al. Fe-doping-induced cation substitution and anion vacancies promoting Co_3O_4 hexagonal nanosheets for efficient overall water splitting. *Mater. Today. Catal.* **2023**, *1*, 100002. DOI
48. Zheng, J.; Sun, R.; Meng, D.; Guo, J.; Wang, Z. Boosting oxygen evolution reaction performance *via* metal defect-induced lattice oxygen redox reactions on spinel oxides. *J. Mater. Chem. A.* **2023**, *11*, 15044-53. DOI
49. Xiao, K.; Wang, Y.; Wu, P.; Hou, L.; Liu, Z. Q. Activating lattice oxygen in spinel $ZnCo_2O_4$ through Filling Oxygen Vacancies with Fluorine for Electrocatalytic Oxygen Evolution. *Angew. Chem. Int. Ed.* **2023**, *62*, e202301408. DOI
50. Zhang, J.; Chen, G.; Sun, D.; et al. Regulating Co-O covalency to manipulate mechanistic transformation for enhancing activity/durability in acidic water oxidation. *Chem. Sci.* **2024**, *15*, 17900-11. DOI
51. Chen, R.; Wang, Z.; Chen, S.; et al. Activating lattice oxygen in spinel oxides via engineering octahedral sites for oxygen evolution. *ACS. Energy. Lett.* **2023**, *8*, 3504-11. DOI
52. Zhu, S.; Wang, X.; Le, J.; et al. Striking stabilization effect of spinel cobalt oxide oxygen evolution electrocatalysts in neutral pH by dual-sites iron incorporation. *Energy. Environ. Mater.* **2024**, *7*, e12594. DOI

53. He, S.; Gao, N.; Zhang, C.; Zhao, L. Halogen modulation in cobalt-manganese oxides for efficient acidic oxygen evolution reaction. *Chem. Eng. J.* **2026**, *531*, 174126. DOI
54. Yan, Q.; Feng, J.; Shi, W.; et al. Chromium-induced high covalent Co-O bonds for efficient anodic catalysts in PEM electrolyzer. *Adv. Sci.* **2024**, *11*, e2402356. DOI
55. Hari Kumar, S. G.; Bozal-Ginesta, C.; Wang, N.; et al. From computational screening to the synthesis of a promising OER catalyst. *Chem. Sci.* **2024**, *15*, 10556-70. DOI PubMed PMC
56. Jeong, I.; Shim, Y.; Oh, S.; et al. A machine learning-enhanced framework for the accelerated development of spinel oxide electrocatalysts. *Adv. Energy. Mater.* **2024**, *14*, 2402342. DOI
57. Sun, Y.; Liao, H.; Wang, J.; et al. Covalency competition dominates the water oxidation structure-activity relationship on spinel oxides. *Nat. Catal.* **2020**, *3*, 554-63. DOI
58. Li, Y.; Zhang, X.; Li, T.; Chen, Y.; Liu, Y.; Feng, L. Accelerating materials discovery for electrocatalytic water oxidation *via* center-environment deep learning in spinel oxides. *J. Mater. Chem. A.* **2024**, *12*, 19362-77. DOI
59. Wang, T.; Sato, N.; Oba, F. Surface reconstruction and band alignment of non-metallic spinel oxides from first principles. *Acta. Mater.* **2025**, *293*, 121034. DOI
60. Guan, D.; Shi, C.; Xu, H.; et al. Simultaneously mastering operando strain and reconstruction effects via phase-segregation strategy for enhanced oxygen-evolving electrocatalysis. *J. Energy. Chem.* **2023**, *82*, 572-80. DOI
61. Chen, Y.; Xu, J.; Jiang, M.; et al. Enhancing oxygen evolution reaction performance: electrochemical activation of the biphasic CoNi/Zn(Fe,Al,Cr)$_2$O$_4$ via controlled aluminum leaching facilitated surface reconstruction. *Adv. Energy. Mater.* **2024**, *14*, 2303450. DOI
62. Li, Z.; Li, B.; Chen, J.; Pang, Q.; Shen, P. Spinel $NiCo_2O_4$ 3-D nanoflowers supported on graphene nanosheets as efficient electrocatalyst for oxygen evolution reaction. *Int. J. Hydrogen. Energy.* **2019**, *44*, 16120-31. DOI
63. Li, Y.; Lin, X.; Du, J. Iron-Facilitated transformation of mesoporous spinel nanosheets into oxyhydroxide active species in the oxygen evolution reaction. *Inorg. Chem.* **2021**, *60*, 19373-80. DOI
64. Davis, E. M.; Bergmann, A.; Kuhlenbeck, H.; Roldan Cuenya, B. Facet dependence of the oxygen evolution reaction on Co_3O_4, $CoFe_2O_4$, and Fe_3O_4 epitaxial film electrocatalysts. *J. Am. Chem. Soc.* **2024**, *146*, 13770-82. DOI PubMed PMC
65. Zhao, C.; Jiang, Z.; Zhang, B.; et al. Unveiling the size and surface effects of spinel Co_3O_4 on the activity of oxygen evolution. *Nano. Today.* **2026**, *68*, 103004. DOI
66. Zuo, S.; Wu, Z. P.; Xu, D.; et al. Local compressive strain-induced anti-corrosion over isolated Ru-decorated Co_3O_4 for efficient acidic oxygen evolution. *Nat. Commun.* **2024**, *15*, 9514. DOI PubMed PMC
67. Feng, Y.; Wang, J.; Feng, K.; et al. Breathing mode in Nd-CoO_x for active and stable proton exchange membrane water electrolysis. *Nat. Commun.* **2025**, *16*, 10998. DOI PubMed PMC
68. Huang, Y.; Zhang, S. L.; Lu, X. F.; Wu, Z. P.; Luan, D.; Lou, X. W. D. Trimetallic spinel $NiCo_{2-x}Fe_xO_4$ nanoboxes for highly efficient electrocatalytic oxygen evolution. *Angew. Chem. Int. Ed.* **2021**, *60*, 11841-6. DOI
69. Yeom, K.; Jo, J.; Shin, H.; et al. Unraveling surface reconstruction during oxygen evolution reaction on the defined spinel oxide surface. *Adv. Funct. Mater.* **2024**, *34*, 2401095. DOI
70. He, B.; Bai, F.; Jain, P.; Li, T. A review of surface reconstruction and transformation of 3d transition-metal (oxy)hydroxides and spinel-type oxides during the oxygen evolution reaction. *Small* **2025**, *21*, e2411479. DOI
71. Huang, K.; Xia, J.; Lu, Y.; et al. Self-reconstructed spinel surface structure enabling the long-term stable hydrogen evolution reaction/oxygen evolution reaction efficiency of FeCoNiRu high-entropy alloyed electrocatalyst. *Adv. Sci.* **2023**, *10*, e2300094. DOI
72. He, B.; Hosseini, P.; Escalera-López, D.; et al. Effects of dynamic surface transformation on the activity and stability of mixed Co-Mn cubic spinel oxides in the oxygen evolution reaction in alkaline media. *Adv. Energy. Mater.* **2025**, *15*, 2403096. DOI
73. Timoshenko, J.; Haase, F. T.; Saddeler, S.; et al. Deciphering the structural and chemical transformations of oxide catalysts during oxygen evolution reaction using quick X-ray absorption spectroscopy and machine learning. *J. Am. Chem. Soc.* **2023**, *145*, 4065-80. DOI PubMed PMC
74. Xiang, W.; Hernandez, S.; Hosseini, P.; et al. Unveiling surface species formed on Ni-Fe spinel oxides during the oxygen evolution reaction at the atomic scale. *Adv. Sci.* **2025**, *12*, e2501967. DOI
75. He, B.; Hosseini, P.; Priamushko, T.; et al. Atomic-scale insights into surface reconstruction and transformation in Co-Cr spinel oxides during the oxygen evolution reaction. *Nat. Commun.* **2025**, *16*, 9895. DOI PubMed PMC
76. Huang, J.; Zhang, Z.; Spezzati, C.; et al. Directly synthesized cobalt oxyhydroxide as an oxygen evolution catalyst in proton exchange membrane water electrolyzers. *Nat. Commun.* **2025**, *16*, 7518. DOI PubMed PMC
77. Xu, Z.; Liu, J.; Luo, Z.; et al. Fundamentals of surface reconstruction and its interplay with oxygen evolution reaction: insights from spinel oxides. *Coord. Chem. Rev.* **2027**, *571*, 218626. DOI

78. Sun, Y.; Wang, J.; Xi, S.; et al. Navigating surface reconstruction of spinel oxides for electrochemical water oxidation. *Nat. Commun.* **2023**, *14*, 2467. DOI PubMed PMC
79. Qiu, C.; Maroun, F.; Bouvier, M.; et al. *Operando* surface X-ray diffraction studies of epitaxial Co_3O_4 and CoOOH thin films during oxygen evolution: pH dependence. *ChemCatChem* **2024**, *16*, e202400988. DOI
80. Haase, F. T.; Ortega, E.; Saddeler, S.; et al. Role of Fe decoration on the oxygen evolving state of Co_3O_4 nanocatalysts. *Energy. Environ. Sci.* **2024**, *17*, 2046-58. DOI
81. Scharf, C. H.; Chandraraj, A.; Dyk, K.; et al. Role of defects in reversible surface restructuring and activity of Co_3O_4 oxygen evolution electrocatalysts. *ACS. Catal.* **2026**, *16*, 4877-91. DOI
82. Duan, Y.; Lee, J. Y.; Xi, S.; et al. Anodic oxidation enabled cation leaching for promoting surface reconstruction in water oxidation. *Angew. Chem. Int. Ed.* **2021**, *60*, 7418-25. DOI
83. Arumugam, B.; Mannu, P.; Darman, R. K.; et al. Unraveling surface reconstruction of MOF-derived La, P-Co_3O_4 for energy-efficient water and urea electrolysis. *Small. Methods.* **2026**, *10*, e2500938. DOI
84. Tran-Phu, T.; Chatti, M.; Leverett, J.; et al. Understanding the Role of (W, Mo, Sb) dopants in the catalyst evolution and activity enhancement of Co_3O_4 during water electrolysis via in situ spectroelectrochemical techniques. *Small* **2023**, *19*, e2208074. DOI
85. van Limpt, R. T. M.; Lao, M.; Tsampas, M. N.; Creatore, M. Unraveling the role of the stoichiometry of atomic layer deposited nickel cobalt oxides on the oxygen evolution reaction. *Adv. Sci.* **2024**, *11*, e2405188. DOI
86. Wang, H.; Lei, J.; Wu, J.; et al. Sustainable water oxidation enabled by a complex-doped cobalt oxide electrode. *Nat. Commun.* **2025**, *17*, 1302. DOI PubMed PMC
87. Bo, S.; Zhang, X.; Wang, C.; et al. Inorganic-organic hybrid cobalt spinel oxides for catalyzing the oxygen evolution reaction. *Nat. Commun.* **2025**, *16*, 2483. DOI
88. Sugawara, Y.; Iwase, K.; Iimura, R.; et al. Ultrasmall manganese nanospinels produced via an alcohol reduction method and their electrocatalytic oxygen evolution reactivity. *ACS. Appl. Mater. Interfaces.* **2025**, *17*, 22487-97. DOI PubMed PMC
89. Zhu, Y.; Cai, T.; Rui, H.; et al. Phosphorus-induced reconstruction of Sub-2 nm ultrafine spinel type CoO nanosheets for efficient water oxidation. *J. Alloys. Compd.* **2021**, *889*, 161704. DOI
90. Zhang, Z.; Jia, C.; Ma, P.; et al. Distance effect of single atoms on stability of cobalt oxide catalysts for acidic oxygen evolution. *Nat. Commun.* **2024**, *15*, 1767. DOI PubMed PMC
91. Wang, M.; Feng, X.; Li, S.; et al. Spinel-type metal oxides with tailored amorphous/crystalline heterointerfaces for enhanced electrocatalytic water splitting. *Adv. Funct. Mater.* **2024**, *34*, 2410439. DOI
92. Fu, L.; Zhou, J.; Kang, Y.; et al. Double-shell structured mixed-spinel oxides for highly efficient oxygen evolution. *Chem. Eng. J.* **2025**, *510*, 161462. DOI
93. Wang, L.; Yuan, C.; Li, C.; et al. Interfacial built-in electric field and interatomic charge transfer synergistically boosting oxygen evolution on CeO_2/Ce-Co_3O_4 electrocatalyst. *Adv. Funct. Mater.* **2025**, *35*, 2502122. DOI
94. Wu, H.; Wang, Z.; Shi, Y.; et al. Constructing a medium-entropy spinel oxide $FeNiMnO_4$/CeO_2 heterojunction as a high-performance electrocatalyst for the oxygen evolution reaction. *Inorg. Chem. Front.* **2024**, *11*, 3786-98. DOI
95. Wan, X.; Wang, C.; Fang, R.; et al. Surface engineering modulation unlocks durable acidic oxygen evolution catalysis in Co_3O_4. *ACS. Catal.* **2026**, *16*, 8750-62. DOI
96. Yu, C.; Du, C.; Ouyang, T.; Zhang, X.; Liu, Z. Silver-induced adsorption optimization of adjacent Co tetrahedral sites for enhanced oxygen reduction/evolution reaction. *Chem. Eng. J.* **2023**, *477*, 147295. DOI
97. Zhang, Q.; Hu, Y.; Wu, H.; et al. Entropy-stabilized multicomponent porous spinel nanowires of $NiFeXO_4$ (X = Fe, Ni, Al, Mo, Co, Cr) for efficient and durable electrocatalytic oxygen evolution reaction in alkaline medium. *ACS. Nano.* **2023**, *17*, 1485-94. DOI
98. Hou, G.; Jia, X.; Kang, H.; et al. CoNi nano-alloys modified yolk-shell structure carbon cage via Saccharomycetes as carbon template for efficient oxygen evolution reaction. *Appl. Catal. B. Environ.* **2022**, *315*, 121551. DOI
99. Yuan, A.; Wang, B.; Guo, M.; et al. Concurrently boosted oxygen reduction/evolution electrocatalysis over highly loaded CoNi/onion-like carbon hybrid nanosheets. *J. Colloid. Interface. Sci.* **2024**, *675*, 602-13. DOI
100. Hu, H.; Zhang, M.; Jiang, M.; Cui, Y.; Gao, X.; Chen, Z. Fe_3O_4-induced interfacial magneto-electronic synergy in yolk-shell nanocages for industrial-level water oxidation. *Chem. Eng. J.* **2025**, *523*, 168684. DOI
101. Wang, Y.; Qin, Y.; Liu, S.; et al. Mesoporous single-crystalline particles as robust and efficient acidic oxygen evolution catalysts. *J. Am. Chem. Soc.* **2025**, *147*, 13345-55. DOI PubMed PMC
102. Pei, C.; Li, N.; Han, X.; et al. Edge-specific confined construction of an interfacial Re-O-Co Bridge for Enhanced Trifunctional Electrocatalysis. *ACS. Nano.* **2025**, *19*, 17674-85. DOI
103. Guo, J.; Wang, R.; Li, J.; et al. Water dissociation: a new dimension for understanding and designing aqueous electrocatalysts. *Adv. Mater.* **2026**, e72916. DOI

104. Gan, R.; Zhao, Q.; Ran, Y.; et al. Regulating interfacial microenvironment via anion adsorption to boost oxygen evolution reaction. *J. Colloid. Interface. Sci.* **2025**, *687*, 724-32. DOI
105. Moon, H.; Son, N.; Goh, M. S.; et al. Auto-selective reaction mechanism on Al-substituted $ZnFe_2O_4$ spinel electrode and sustainable water oxidation by oxygen vacancy transition. *Appl. Surf. Sci.* **2023**, *632*, 157553. DOI
106. Cheng, J.; Zhang, Z.; Li, X.; et al. High-entropy spinel oxide nanoparticles with surface anionic Mo species for seawater oxidation. *ACS. Appl. Nano. Mater.* **2025**, *8*, 14999-5007. DOI
107. Guo, J.; Zheng, Y.; Hu, Z.; et al. Direct seawater electrolysis by adjusting the local reaction environment of a catalyst. *Nat. Energy.* **2023**, *8*, 264-72. DOI
108. Nguyen, T. X.; Shih, T.; Tran, N. T. T.; et al. Chlorine-resistant high-entropy spinel oxide catalyst for efficient and durable seawater anion exchange membrane water electrolysis. *Chem. Eng. J.* **2026**, *534*, 174932. DOI
109. Wu, L.; Zhao, B.; Huang, W.; et al. Dynamic chromium dopant promotes interfacial water activation on cobalt spinel oxide for efficient oxygen evolution in acid. *Nat. Commun.* **2026**, *17*, 2598. DOI PubMed PMC
110. Krishnan, A. V.; Saini, K.; Enriquez, L. G.; Ramana, C. V.; Sreenivasan, S. T. Lewis acid site engineering in chromite spinels orchestrated surface reconstruction and surpasses RuO_2 in oxygen evolution. *Small* **2025**, *21*, e08245. DOI PubMed
111. Hu, W.; Zhang, J.; Fan, Y.; et al. Regulating surface hydroxyl groups in CoO_x via atomically dispersed ru for durable acidic oxygen evolution. *J. Am. Chem. Soc.* **2026**, *148*, 16267-77. DOI
112. Wang, Y.; Jia, B.; Qin, W.; et al. High-density W single atoms in two-dimensional spinel oxide break the structural integrity for enhanced oxygen evolution catalysis. *J. Am. Chem. Soc.* **2025**, *147*, 32249-62. DOI
113. Yang, H.; Chen, F.; Wang, X.; et al. Self-reconstructed spinel with enhanced SO_4^{2-} adsorption and highly exposed Co^{3+} from heterostructure boosts activity and stability at high current density for overall water splitting. *Adv. Funct. Mater.* **2025**, *35*, 2419978. DOI

Disclaimer/Publisher's Note: All statements, opinions, and data contained in this publication are solely those of the individual author(s) and contributor(s) and do not necessarily reflect those of OAE and/or the editor(s). OAE and/or the editor(s) disclaim any responsibility for harm to persons or property resulting from the use of any ideas, methods, instructions, or products mentioned in the content.

© The Author(s) 2026. Open Access This article is licensed under a Creative Commons Attribution 4.0 International License (https://creativecommons.org/licenses/by/4.0/), which permits unrestricted use, sharing, adaptation, distribution and reproduction in any medium or format, for any purpose, even commercially, as long as you give appropriate credit to the original author(s) and the source, provide a link to the Creative Commons license, and indicate if changes were made.